Dynamics of A Three-Variable Nonlinear Model of Vasomotion: Comparison of Theory and Experiment

D. Parthimos,* R. E. Haddock,† C. E. Hill,† and T. M. Griffith*
*Wales Heart Research Institute, Department of Diagnostic Radiology, Cardiff University, Cardiff, United Kingdom; and †Division of Neuroscience, John Curtin School of Medical Research, Australian National University, Canberra, Australia

ABSTRACT The effects of pharmacological interventions that modulate Ca^{2+} homeodynamics and membrane potential in rat isolated cerebral vessels during vasomotion (i.e., rhythmic fluctuations in arterial diameter) were simulated by a third-order system of nonlinear differential equations. Independent control variables employed in the model were $[Ca^{2+}]$ in the cytosol, $[Ca^{2+}]$ in intracellular stores, and smooth muscle membrane potential. Interactions between ryanodine- and inositol 1,4,5-trisphosphate-sensitive intracellular Ca^{2+} stores and transmembrane ion fluxes via K^+ channels, Cl^- channels, and voltage-operated Ca^{2+} channels were studied by comparing simulations of oscillatory behavior with experimental measurements of membrane potential, intracellular free $[Ca^{2+}]$ and vessel diameter during a range of pharmacological interventions. The main conclusion of the study is that a general model of vasomotion that predicts experimental data can be constructed by a low-order system that incorporates nonlinear interactions between dynamical control variables.

INTRODUCTION

Blood flow and tissue perfusion normally exhibit a high degree of temporal variability that is not simply attributable to fluctuations in heart rate and blood pressure. An important contributory mechanism is the rhythmic vascular contractile activity that is ubiquitous in arterioles, resistance arteries, and conduit arteries—a phenomenon known as vasomotion. Although the physiological benefits of vasomotion remain controversial, time-dependent regional redistributions in microvascular flow ensure that all tissue elements ultimately receive perfusion, and it has also been suggested that the phenomenon represents an adaptive response because it is enhanced in hemorrhagic shock and may then serve to preserve tissue viability (reviewed in 1–3). Rhythmic activity may also be observed in isolated arteries, both spontaneously and after stimulation with constrictor agonists in otherwise quiescent vessels (4–8). At the cellular level, vasomotion is associated with oscillations in $[Ca^{2+}]_i$ and membrane potential, with uncoordinated fluctuations in $[Ca^{2+}]_i$ in individual smooth muscle cells becoming almost synchronous at the onset of large-scale oscillatory activity (7–13). The mechanisms that underpin such entrainment involve electrical and/or chemical coupling via gap junctions, since pharmacological interruption of direct cell-cell communication suppresses rhythmic contractile activity in isolated arterial segments (6,13,14).

In isolated rabbit and rat arteries, vasomotion often exhibits patterns of behavior that are generic in nonlinear systems, including period-doubling, quasiperiodic, and intermittent routes for the transition from regular to chaotic behavior (5,15–19). Nonlinear statistical techniques have provided estimates of the minimum number of underlying dynamic control variables that contribute to vasomotion, and in rabbit and rat arteries these generally give a value between 2 and 3, both in vitro and in vivo, with a value between 3 and 4 sometimes being obtained (1,5,16,20). Although we have previously shown that a four-variable mathematical model incorporating nonlinear interactions between the ion transport systems that regulate arterial tone can successfully simulate complex chaotic patterns of response in isolated rabbit arteries (17), the predominance of low dimensional behavior suggests that in many situations a three-variable model could suffice to reproduce the general patterns of vasomotion observed experimentally. In this study, we therefore investigated the behavior of a model that employs $[Ca^{2+}]$ in the cytosol, $[Ca^{2+}]$ in intracellular stores, and membrane potential as the dominant control variables to define the minimal components that can be used to model vasomotion. In our previous model, regenerative intracellular Ca^{2+}-induced Ca^{2+} release was assumed to be mediated exclusively via the ryanodine receptor (RyR), and a coexisting inositol 1,4,5-trisphosphate ($InsP_3$)-sensitive store was assumed to provide a steady flux of Ca^{2+} into the cytosol. In this model, we now incorporate a second Ca^{2+}-induced Ca^{2+} release mechanism via the inositol 1,4,5-trisphosphate receptor ($InsP_3R$). This approach allows evaluation of the dynamical consequences of differences in the kinetics of the RyR and $InsP_3R$ and interactions between the two channels can be studied by varying their relative contributions to intracellular Ca^{2+} movements.

The results of simulations were compared with the effects of pharmacological interventions in the rat basilar artery and its branches, in which rhythmic activity is observed spontaneously

Submitted February 9, 2007, and accepted for publication April 20, 2007.

Address reprint requests to Professor T. M. Griffith, Wales Heart Research Institute, Dept. of Diagnostic Radiology, Cardiff University, Heath Park, Cardiff, CF14 4XN, UK. Tel.: 44-2920–743070; Fax: 44-2920–744726; E-mail: Griffith@Cardiff.ac.uk.

Editor: Dorothy A. Hanck.

0006-3495/07/09/1534/23 $2.00

doi: 10.1529/biophysj.107.106278

and does not require the application of an exogenous constrictor agonist. Experimental data consisted of electrophysiological measurements of membrane potential and ratiometric imaging of smooth-muscle $[Ca^{2+}]_i$, with changes in vessel diameter continuously monitored by videomicroscopy. Two of the key control variables of the system were therefore directly observable, thus allowing detailed validation of the dynamical contributions of the individual model components. The model successfully reproduced the effects of a broad range of pharmacological interventions and allowed clarification of the different routes through which agents that affect $[Ca^{2+}]_i$ and membrane potential modulate vasomotion.

METHODS

Experimental methods

All experiments were performed in accordance with institutional guidelines using male Wistar rats (14–17 days postnatal) that were anaesthetized with ether and decapitated. After removal of the brain into cold (5–7°C) dissection buffer containing (mM) 3 3-(*N*-morpholino)propanesulphonic acid (Mops), 1.2 NaH_2PO_4, 4.6 glucose, 2 pyruvate, 0.02 EDTA(Na), 0.15 albumin, 145 NaCl, 4.7 KCl, 2 $CaCl_2$, and 1.2 $MgSO_4$, a rectangular section of the meninges containing the basilar artery and its primary and secondary branches was isolated. The preparation was pinned to the bottom of a 1-ml recording chamber which was perfused at a constant flow rate (3 ml min^{-1}) with Krebs solution containing (mM) 120 NaCl, 5 KCl, 25 $NaHCO_3$, 1 NaH_2PO_4, 2.5 $CaCl_2$, 2 $MgCl_2$, and 11 glucose, gassed with 95% O_2 and 5% CO_2 and maintained at 33–34°C.

Measurements of membrane voltage and vasomotion

An individual primary or secondary branch of the basilar artery was visualized by videomicroscopy and the diameter of the vessel continuously monitored (Diamtrak (21)). After 20 min of superfusion with Krebs solution, spontaneous contractions were routinely recorded in all arteries and arterioles. Smooth muscle cells were impaled with sharp microelectrodes filled with 0.5 M KCl (tip resistance 120–220 M Ω), and membrane potential records were amplified with an Axoclamp 2B (Axon Instruments, Foster City, CA). Changes in membrane potential and changes in vessel diameter in the same region were simultaneously recorded. After measurements in control Krebs solution, preparations were incubated in drugs up to a maximum period of 30 min before being returned to control solution.

Measurements of intracellular calcium

In experiments in which changes in intracellular calcium concentration were made, a small area of the meninges surrounding the primary and secondary arteries was gently removed and the preparations incubated at room temperature (22°C) in modified Krebs solution containing reduced calcium (0.5 mM $CaCl_2$), the detergent pluronic F-127 (0.01%), and the ratiometric fluorescent dye Fura-2 acetoxymethyl ester (5 μM) for 40 min. This was followed by superfusion with warmed (34°C) Krebs solution, containing 2.5 mM $CaCl_2$ for 20 min. When viewed with 380 nm light at this time, only the outer layer of smooth muscle cells could be visualized and no endothelial cells were ever seen to be fluorescent. No smooth muscle cells were loaded if the meninges were left in place. Measurements of calcium were made in individual smooth muscle cells or within an area of the vascular wall by calculating the ratio of the fluorescence emission recorded at 510 nm after sequential excitation of the preparation with 340 and 380 nm light ($F_{340/380}$; Polychrome II illumination system; TILL Photonics, Gräfelfing, Germany). In the case of changes in calcium in the arterial wall, measurements were made at 30 Hz with a photometry system (TILL Photonics) and recorded with pCLAMP 8 (Axon Instruments). In the case of changes in $[Ca^{2+}]$ in individual smooth muscle cells, images were captured at 4 Hz using an intensified cooled CCD camera (Princeton Instruments, Trenton, NJ) and data processed using Axon Imaging Workbench (Axon Instruments). Simultaneous measurement of vessel diameter was made possible by continuous image capture under infrared illumination (775 nm; Hamamatsu Performance Vidicon camera, Hamamatsu City, Japan). To restrict exposure of the preparation to ultraviolet light, measurements of calcium were made in control Krebs solution, immediately after the equilibration period, and after drugs had been present for 20 min.

Drugs and solutions

Drugs used were obtained from the following sources: 1-(6-((17β-3-methoxyestra-1,3,5(10)-trien-17-yl) amino)-hexyl)-1*H*-pyrrole-2,5-dione (U73122), nifedipine, 2-hydroxyethanesulfonic acid (sodium isethionate), niflumic acid, charybdotoxin (Sigma Chemical, St. Louis, MO); Fura-2 acetoxymethyl ester, pluronic acid (Molecular Probes, Eugene, OR); ryanodine (Biomol, Plymouth Meeting, PA). U73122 and niflumic acid were dissolved in DMSO as 10^4-fold stock solutions and diluted into Krebs solution. Nifedipine was similarly dissolved in ethanol (10^4-fold stock) and charybdotoxin was dissolved in PBS containing 0.1% BSA as a 10^3-fold stock. All other drugs were made up as 10^3-fold stock solutions in distilled water and diluted into Krebs solution.

Formulation of the mathematical model

The model is based on an intracellular Ca^{2+} oscillator that generates oscillatory activity via cyclical Ca^{2+}-induced Ca^{2+} release (CICR) from internal stores located in the sarcoplasmic reticulum (SR). Since Ca^{2+} released into the cytosol is pumped out of the cell as well as being resequestered by the intracellular store via the SERCA pump, sustained oscillatory activity will have an obligatory requirement for influx of extracellular Ca^{2+}, so the intracellular oscillator is intimately coupled with Ca^{2+} fluxes across the plasma membrane. Cytochemical evidence indicates that the RyR and the $InsP_3R$ are both present on the SR of vascular myocytes and distributed throughout their cytoplasm (22–24). Although the spatial overlap of RyR- and $InsP_3R$-gated stores may not always be complete (25), for simplicity we have assumed that they mediate CICR from a common intracellular Ca^{2+} store. This allows the development of a 1-pool, 2-receptor representation of the intracellular Ca^{2+} oscillator that can be described mathematically by just two variables, namely $[Ca^{2+}]$ in the cytosol and $[Ca^{2+}]$ in the lumen of the common store (x and y, respectively, in Eqs. 1 and 2).

Three RyR subtypes are expressed in vascular smooth muscle (22,26) and each subtype exhibits low-affinity inhibition by Ca^{2+} such that RyR1 channels close when $[Ca^{2+}]$ approaches 1 mM, and RyR2 and RyR3 channels close when $[Ca^{2+}]$ is in the range 1–10 mM (27,28). Since such Ca^{2+} concentrations may be supraphysiological, even in localized intracellular domains, the extent to which Ca^{2+}-dependent inactivation of the receptor by cytosolic Ca^{2+} serves as a negative control mechanism that contributes to the termination of RyR-mediated CICR is unclear. Consequently, in formulating the model it was assumed that there is a negligible fall off in the open probability of the receptor at $[Ca^{2+}]$ levels within the physiological range. Activation of the RyR by Ca^{2+} occurs within ~1 ms, and the channel rapidly turns off (i.e., deactivates) with a time constant of 5–6 ms in response to fast reductions in $[Ca^{2+}]$ (27). The RyR also exhibits a so-called ''adaptive'' inactivation to elevations in $[Ca^{2+}]$ that allows subsequent increases in $[Ca^{2+}]$ to elicit nearly identical increases in open probability (27), and in the case of RyR2 such adaptation occurs within milliseconds in the presence of physiological concentrations of the Mg^{2+} ion (29). Since the kinetics of the

RyR is rapid compared to the timescale of vasomotion (i.e., seconds to minutes (1)), it was assumed that its open probability is dominated by instantaneous activation and deactivation, and time-dependent inactivation and adaptation of the receptor were not specifically incorporated in the model. Based on arguments outlined in the literature (30–32), the steady-state $[Ca^{2+}]$ dependence of the RyR was generally modeled as a monotonically increasing fourth-order Hill sigmoidal (Fig. 1 *A*). This is consistent with the tetrameric nature of the RyR protein, although it should be noted that under different experimental conditions the degree of cooperativity implied by the Hill coefficient can lie between 2 and 7 (28,33,34). In some simulations, therefore, the value of this coefficient was varied systematically to assess its dynamical role. Ca^{2+} concentrations resulting in half-maximal activation of the RyR were varied between 0.2 and 0.9 μM to encompass the range of values reported in the literature (27,28,33). No attempt was made to allow for differences in the gating characteristics of the three RyR subtypes or spatial heterogeneity in their possible subcellular location (22,26).

Three $InsP_3R$ subtypes have been identified in vascular smooth muscle cells and are generally reported to exhibit biphasic steady-state activation curves as a function of $[Ca^{2+}]$ under different experimental conditions (24,35–38). In superfusion studies with isolated microsomes, the peak $InsP_3R$ open probability attained after elevations in $[Ca^{2+}]$ decreases to a steady plateau over 0.5–2 s through Ca^{2+}-dependent and Ca^{2+}-independent inactivation mechanisms that remain poorly understood (39). Indeed, although some studies have suggested that Ca^{2+}-sensitive binding of calmodulin to the $InsP_3R$ facilitates closure of the channel, the $InsP_3R3$ has been reported to exhibit a biphasic activation curve despite the lack of a calmodulin binding domain in this specific subtype (40). The $InsP_3R$ also ''adapts'' to submaximal concentrations of $InsP_3$ that evoke transient rather than continuous Ca^{2+} release, in the sense that subsequent increments in $[InsP_3]$ are capable of eliciting further Ca^{2+}-release transients (41). Complex kinetic binding models have been devised to simulate the characteristics of time-dependent inactivation and adaptation of the $InsP_3R$ (41,42). However, Li and Rinzel (43) were able to capture the essential dynamical features of this approach by formulating a reduced two-variable model in which a fast variable described Ca^{2+} release and a slow variable described time-dependent inactivation of the $InsP_3R$. Hofer (44) further simplified this scenario by adopting a quasi-steady-state approximation that removed the necessity for a dynamic inactivation variable in hepatocytes, a cell type in which the oscillation period is longer than the time constant for $InsP_3R$ inactivation and ranges from 30 s at maximal levels of stimulation to several minutes for low agonist doses. For the purposes of this study, therefore, activation and deactivation of the $InsP_3R$ by Ca^{2+} ions were assumed to be instantaneous, and time-dependent inactivation and adaptation of the $InsP_3R$ were not incorporated in the model because they generally occur on a timescale faster than that of vasomotion, as noted above. This approach is also consistent with experimental evidence that photolytically induced elevations in $[Ca^{2+}]$ up to ~150 nM cause an immediate potentiation of Ca^{2+} release in permeabilized smooth muscle cells, whereas larger Ca^{2+} jumps (in the range 250–850 nM) cause immediate (rather than delayed) slowing of Ca^{2+} release (45).

The dominant $InsP_3R$ subtype present in the smooth muscle of the rat basilar artery is $InsP_3R1$, with much lower expression of $InsP_3R2$ and no expression of $InsP_3R3$ (24). Empirically, Mak and co-workers (37) found that the quasisteady open probability of $InsP_3R1$ channels could be fitted to a dual sigmoidal Hill function that was hypothesized to reflect the existence of activating sites with a Hill coefficient of 2 and inhibitory sites with a Hill coefficient of 4, thus suggesting that activation and inhibition of the tetrameric $InsP_3R$ by Ca^{2+} are both cooperative events, requiring binding of Ca^{2+} ions to two monomers to promote channel opening and binding of Ca^{2+} to all four components to inhibit channel opening. Subsequent reports have employed an analogous approach to model the quasisteady Ca^{2+} sensitivities of a variety of $InsP_3R$ subtypes (including chimeric constructs), and have reported activating coefficients in the range 1–4 and inactivating coefficients in the range 1–3 (36,38). In this study, dual Hill sigmoidals were used to generate biphasic open probability curves that allow the coefficients of their activation and deactivation components to be varied independently. The positions of the curves could thus be manipulated to encompass experimental evidence that the Ca^{2+} concentrations resulting in 50% activation or inactivation of the $InsP_3R$ channel may lie between 30 nM and 1 μM and between 200 nM and 50 μM, respectively, with corresponding peak values lying in the range 100 nM to 1 μM (36–38) (Fig. 1 *B*). In intact cells, the shape and position of the these curves will be influenced by $[InsP_3]$ and [ATP], which can increase sensitivity to Ca^{2+} and/or remove inhibition by high $[Ca^{2+}]_i$ (36,42), but levels of these factors could not be manipulated experimentally, since all vessels exhibited spontaneous vasomotion.

In previous theoretical studies, the driving force for CICR (via the RyR or the $InsP_3R$) has often been modeled as the concentration gradient between $[Ca^{2+}]$ in the store and the cytosol. However, there is evidence that store depletion itself contributes to the termination of Ca^{2+} release via both the RyR (31,46,47) and the $InsP_3R$ (41,48,49). More specifically, it has been hypothesized that inhibition of the $InsP_3R$ observed when store $[Ca^{2+}]$ is low reflects the binding of regulatory intraluminal proteins such as ERp44 to the receptor. Thus, the interaction of this protein with $InsP_3R1$ is weak when store $[Ca^{2+}]$ exceeds 100 μM, providing a mechanism whereby binding of ERp44 to the receptor could actively diminish Ca^{2+} release (50). Since the open probabilities of the RyR and $InsP_3R$ may thus both decrease when store $[Ca^{2+}]$ is low, a nonlinear fall-off in CICR as store $[Ca^{2+}]$ declines was implicitly incorporated in this model as a sigmoidal function of store $[Ca^{2+}]$.

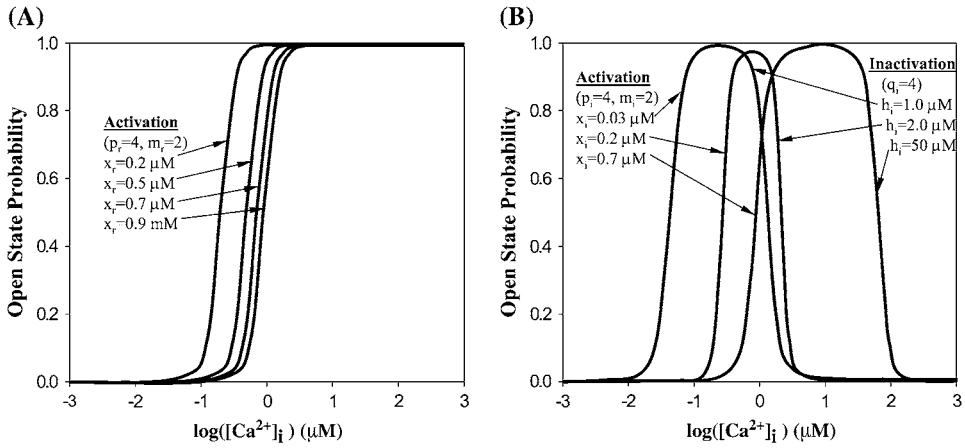

FIGURE 1 Nonscaled steady-state open probability curves. (*A*) The RyR curves are fourth-order Hill sigmoidals whose sensitivity to Ca^{2+} is governed by the coefficient x_r, which defines the concentration producing half-maximal activation of the channel. (*B*) Sample $InsP_3R$ curves plotted for three values of the half-point of the activation sigmoidal (x_i) and three values for the half-point for the inactivation sigmoidal (h_i). The Hill coefficient for both sigmoidals was selected as 4. Parameters were selected to encompass the range of positions of the RyR and $InsP_3R$ curves reported in the literature (see text). In general, the maximum open-state probability of the channels may be <1, but this is accounted for by the scaling coefficients C_r and C_i.

The Hill coefficient for this mechanism was generally taken as 4, although the effects of other values were also investigated. Uptake of Ca^{2+} by the store via the SERCA pump was modeled as a second-order Hill sigmoidal in all simulations, consistent with experimental data (51).

In open cell systems based on CICR, sustained oscillations in Ca^{2+} require an inward flux of extracellular Ca^{2+} into the cytosol to compensate for loss of Ca^{2+}, e.g., via the plasmalemmal Ca^{2+} ATPase and forward-mode Na^+-Ca^{2+} exchange (NCX). In the open model described in this article, such influx is provided via Ca^{2+}-permeable nonselective cation channels (NSCCs), voltage-operated Ca^{2+} channels (VOCCs) and reverse-mode NCX. Recent experimental evidence suggests that NSCCs are constructed from transient receptor potential proteins, and are constitutively active in vascular myocytes, so they may contribute to resting membrane conductance and basal Ca^{2+} influx, in addition to being activated by vasoconstrictor agonists, depletion of Ca^{2+} stores, and mechanical stretch (52). Since NSCCs are gated by diacylglycerol (DAG), via both protein kinase C-dependent and -independent mechanisms (52), a critical determinant of vasomotion may therefore be the mobilization of Ca^{2+} by phospholipase C (PLC), since this enzyme underpins the formation of both DAG and $InsP_3$ and may therefore simultaneously regulate extracellular Ca^{2+} influx and Ca^{2+} release from stores via the $InsP_3R$ (53).

The third variable incorporated in the model is membrane potential (z in Eq. 3), with influx of Ca^{2+} ions via VOCCs being promoted by membrane depolarization. Membrane potential is also influenced by the balance between K^+ and Cl^- movements, which compete to drive cell potential toward their respective reversal potentials at approximately −95 and −25 mV, and by NCX, depending on whether the exchanger operates in forward or reverse mode. To simplify computation, the quasisteady open probability of these electrogenic membrane ion transport systems was assumed to govern their contribution to membrane potential. This approach differs from a previous model of arterial vasomotion in which the open-state probability of K^+ channels was assigned the status of an independent dynamical variable that exhibited time-dependent inactivation (17).

The third-order system of coupled nonlinear differential equations describing this open system assumes the following form:

Cytosolic free Ca^{2+}:

$$\frac{dx}{dt} = A - G_{Ca}\frac{z - z_{Ca_1}}{1 + e^{-(z - z_{Ca_2})/R_{Ca}}} + G_{Na/Ca}\frac{x}{x + x_{Na/Ca}}(z - z_{Na/Ca}) - B\frac{x^n}{x^n + x_b^n}$$

Ca^{2+} influx via NSCC; Ca^{2+} influx via VOCC; NCX; SR uptake

$$+ C_r\frac{y^{m_r}}{y^{m_r} + y_r^{m_r}}\frac{x^{p_r}}{x^{p_r} + x_r^{p_r}} + C_i\frac{y^{m_i}}{y^{m_i} + y_i^{m_i}}\frac{x^{p_i}}{x^{p_i} + x_i^{p_i}}\left(1 - \frac{x^{q_i}}{x^{q_i} + h_i^{q_i}}\right)$$

CICR via RyR; CICR via $InsP_3R$

$$- Dx^k\left(1 + \frac{z - z_d}{R_d}\right) + Ly$$

Ca^{2+} extrusion; SR leak (1)

$[Ca^{2+}]$ in the sarcoplasmic reticulum:

$$\frac{dy}{dt} = B\frac{x^n}{x^n + x_b^n} - C_r\frac{y^{m_r}}{y^{m_r} + y_r^{m_r}}\frac{x^{p_r}}{x^{p_r} + x_r^{p_r}} - C_i\frac{y^{m_i}}{y^{m_i} + y_i^{m_i}}\frac{x^{p_i}}{x^{p_i} + x_i^{p_i}}\left(1 - \frac{x^{q_i}}{x^{q_i} + h_i^{q_i}}\right) - Ly \quad (2)$$

SR uptake; CICR via RyR; CICR via $InsP_3R$; SR leak

Relationship between membrane ion fluxes and cell potential:

$$\frac{dz}{dt} = \gamma\left(-G_{Cl}\frac{x}{x + x_{Cl}}(z - z_{Cl}) - 2G_{Ca}\frac{z - z_{Ca_1}}{1 + e^{-(z - z_{Ca_2})/R_{Ca}}} - \right.$$

Cl^- channels; Ca^{2+} influx via VOCC

$$\left. - G_{Na/Ca}\frac{x}{x + x_{Na/Ca}}(z - z_{Na/Ca}) - G_K(z - z_K)\frac{x}{x + \beta e^{-(z - z_{Ca_3})/R_K}}\right) \quad (3)$$

NCX; K^+ efflux

The reversal potential of the Na^+-Ca^{2+} exchange mechanism is $[Ca^{2+}]_i$-dependent and can be calculated as $z_{Na/Ca} = 3z_{Na} - 2z_{Ca1}$, where the reversal potentials z_{Ca1} and z_{Na} are derived from the Nernst equation according to $z_{Ca1} = (RT)/(FZ_{Ca})\ln([Ca^{2+}]_o)/([Ca^{2+}]_i)$ and $z_{Na} = (RT)/(FZ_{Na})\ln([Na^+]_o)/([Na^+]_i)$ with $Z_{Na} = 1$, $Z_{Ca} = 2$, and $(RT)/(F) = 0.024$ (R, gas constant; F, Faraday's constant, $T = 310$°K). It was assumed that $[Ca^{2+}]_o = 2.5$ mM and $(3RT)/(FZ_{Na})\ln([Na^+]_o)/([Na^+]_i) = 0.207$.

The coefficient γ represents a scaling factor that determines the rate at which ionic currents modulate variations in membrane potential (17). Realistic responses that matched experimental data were obtained by fixing the value of γ at 1 V/μM throughout the study. Ca^{2+} ions in the cytosol and

the SR are bound by intracellular proteins to different extents, so for the purposes of modeling it is necessary to define ''effective volumes'' that are distinct from the physical volumes of the cytosol and the SR. As argued in Parthimos et al. (17), the effective volumes of the two compartments are closely similar, thus permitting the assumption that Ca^{2+} concentration changes in the cytosol and stores are directly related, as is implicit in Eqs. 1 and 2.

Insights into the contribution of CICR via the RyR and $InsP_3R$ to the dynamics of the model were obtained by plotting the x and y nullclines, i.e., the loci of points at which the rates of change of $[Ca^{2+}]_i$ and $[Ca^{2+}]_{SR}$ are both zero under different parametric conditions. Standard stability theory indicates that oscillations occur only when the eigenvalues that characterize the deformation of the phase space in the neighborhood of the crossing of these nullclines are complex conjugates with a positive real part, and for the generic form of the nullclines generated by Eqs. 1 and 2 this condition requires that both exhibit a negative slope at the point of intersection (17). The limit cycle oscillation that emerges around the unstable equilibrium point then exhibits three distinct phases. These include a section that determines the amplitude of the oscillatory behavior and in which CICR causes rapid emptying of the SR Ca^{2+}store leading to an abrupt rise in $[Ca^{2+}]_i$ and fall in $[Ca^{2+}]_{SR}$. This is followed by a section in which Ca^{2+} ions are extruded from the cell more rapidly than they enter from the extracellular space, so that $[Ca^{2+}]_i$ declines and $[Ca^{2+}]_{SR}$ remains low. Eventually, however, influx of Ca^{2+} dominates over extrusion, allowing sequestration of Ca^{2+} entering the cell within the SR store, with $[Ca^{2+}]_i$ remaining almost constant. Store refilling continues until the driving force for CICR once again increases to the point where regenerative Ca^{2+} release is able to initiate another cycle (17,30). The overall period of the resulting oscillatory behavior is governed by the duration of store refilling, since this is slow compared to the other two components of the cycle.

Numerical methods

Simulations were produced by numerical integration with the Runge-Kutta-Merson algorithm, employing an integration step in the range of 0.0005–0.003 s. Physiological values for fixed coefficients employed in the simulations were taken from Parthimos et al. (17) and are provided in Table 1. Pharmacological interventions were simulated by altering the appropriate coefficient(s) in Eqs. 1–3 in a stepwise fashion according to the ion transport system under study, as indicated in the corresponding figure or figure legend.

RESULTS

Control responses

Spontaneous oscillations in the membrane potential of the rat basilar artery and its primary branches were of the order of 5–15 mV, generally falling within the membrane potential range –30 to –45 mV, with oscillations in diameter being 5–10% of mean.

Role of CICR

Effects of ryanodine

Ryanodine has variously been reported to promote opening of the RyR channel with preserved or decreased single-channel conductance, to increase the Ca^{2+} sensitivity of the channel, to lock the channel in an open subconductance state, or to cause complete channel closure (28,54,55). These effects of ryanodine were simulated with C_i set to zero (i.e., in the absence of $InsP_3R$-mediated Ca^{2+} release) as follows:

1. Increases in the coefficient C_r were used to scale the single-channel open-probability curve and thus increase Ca^{2+} flux from the SR store (i.e., number of RyR channels × channel conductance × open probability). This strategy resulted in a decrease in the amplitude of oscillations in membrane potential and $[Ca^{2+}]_i$ and an increase in oscillation frequency. There was little effect on the mean values of membrane potential and $[Ca^{2+}]_i$ (Fig. 2 *A*).
2. Decreases in the coefficient x_r were used to mimic the enhanced Ca^{2+} sensitivity of the RyR activation sigmoidal reported with low concentrations of ryanodine. This strategy will increase Ca^{2+} flux from the SR store via the RyR and, as in scenario 1, revealed a reciprocal relationship between the amplitude and frequency of oscillations in membrane potential and $[Ca^{2+}]_i$, but no major change in their mean values (Fig. 2 *B*).
3. Increases in the leak coefficient L to simulate the formation of the locked-open subconductance state decreased the amplitude of rhythmic activity without affecting oscillation frequency (Fig. 2 *C*).
4. Decreases in coefficient C_r to mimic the closure of the RyR reported with high micromolar concentrations of ryanodine resulted in an increase in oscillation amplitude and an associated decrease in frequency (Fig. 2 *D*). Mathematically, this is the converse of scenario 1.

Experimentally, 10 μM ryanodine reduced the amplitude of rhythmic activity with little effect on mean diameter, membrane potential, wall $[Ca^{2+}]_i$, or $[Ca^{2+}]_i$ in individual smooth-muscle cells (Fig. 2, *E–G*). Since this action of ryanodine was generally associated with an increase in oscillation frequency, it follows that the observed effects of ryanodine in the rat basilar artery were most closely modeled by increasing the Ca^{2+} flux via the RyR as in scenarios 1 and 2 above.

Detailed insights into the dynamics of the CICR mechanism were obtained by nullcline analysis in which two-dimensional plots of x against y were generated with the value of z held constant at −40 mV. On increasing C_r or reducing x_r, the intersection of x and y nullclines translated downward with a progressive decrease in the size of the limit cycle encircling the unstable equilibrium point (Fig. 3, *A* and *B*). Conversely, the decreases in C_r that model channel closure increased the size of the limit cycle (Fig. 3 *A*). Oscillatory behavior ceased for extreme values of C_r or x_r, where the equilibrium point became stable. Increases in L had a relatively small effect on the position of the intersection of the x and y nullclines (Fig. 3 *C*). Consequently, the duration of the slow SR refilling phase of the limit cycle, and thus oscillation frequency, was not strongly dependent on L, whereas the amplitude of the oscillation decreased as the fast emptying phase of the limit cycle became abbreviated for high values of L. The general relationship between the amplitude and frequency of vasomotion during these different

TABLE 1 Table of coefficients

Parameter	Description	Value (unless otherwise stated)
A	Ca^{2+} influx via NSCCs. Simulations,	2.3 μM/s
	Nullcline analysis	0.7 μM/s
G_{Ca}	whole-cell conductance for voltage-operated Ca^{2+} channels	12 μM/V s
z_{Ca1}	reversal potential for VOCC	120–135 mV
z_{Ca2}	half point of the VOCC activation sigmoidal	−24 mV
R_{Ca}	maximum slope of the VOCC activation sigmoidal	8.5 mV
$G_{Na/Ca}$	whole-cell conductance for NCX	43.8 μM/V s
$x_{Na/Ca}$	half-point for activation of NCX by Ca^{2+}	0.5 μM
$z_{Na/Ca}$	reversal potential for NCX	−30 to −45 mV
B	SR uptake rate constant	400 μM s^{-1}
x_b	half-point of the SR ATPase activation sigmoidal	4.4 μM
n	Hill coefficient for x dependence of SR uptake	2
C_r	Ca^{2+}-induced Ca^{2+} release rate constant for RyR	1250 μM s^{-1}
C_i	Ca^{2+}-induced Ca^{2+} release rate constant for $InsP_3R$	0 μM s^{-1}
y_r	half-point of the CICR via RyR Ca^{2+} efflux sigmoidal	8.9 μM
x_r	half-point of the RyR CICR activation sigmoidal	0.9 μM
p_r	Hill coefficient for x dependence of CICR via RyR	4
m_r	Hill coefficient for y dependence of CICR via RyR	2
y_i	half-point of the CICR via $InsP_3R$ Ca^{2+} efflux sigmoidal	8.9 μM
x_i	half-point of the $InsP_3R$ CICR activation sigmoidal	0.03–0.9 μM
p_i	activation Hill coefficient for x dependence of CICR via $InsP_3R$	4
m_i	Hill coefficient for y dependence of CICR via $InsP_3R$	2
h_i	half-point of the $InsP_3R$ CICR inactivation sigmoidal	1.0–20 μM
q_i	inactivation Hill coefficient for x dependence of CICR via $InsP_3R$	4
D	rate constant for Ca^{2+} extrusion by the ATPase pump	6.25 μM^{-1} s^{-1}
k	exponent for x dependence of Ca^{2+} extrusion	2
z_d	intercept of voltage dependence of extrusion ATPase	−100 mV
R_d	slope of voltage dependence of extrusion ATPase	250 mV
L	leak from SR rate constant	0.025 s^{-1}
γ	scaling factor relating net movement of ion fluxes to membrane voltage (inversely related to cell capacitance)	1 V/μM
G_{Cl}	whole-cell conductance for Cl^- current	65 μM/V s
z_{Cl}	reversal potential for Cl^- channels	−25 mV
x_{Cl}	Ca^{2+} sensitivity of Cl^- channels	0 μM
G_K	whole-cell conductance for K^+ efflux	43 μM/V s
z_K	reversal potential for K^+	−95 mV
β	Ca^{2+} sensitivity of K_{Ca} channel activation sigmoidal	0 μM
z_{Ca3}	half-point for the K_{Ca} channel activation sigmoidal	−27 mV
R_K	maximum slope of the K_{Ca} activation sigmoidal	12 mV

approaches to simulation was explored systematically (Fig. 3 *D*). It can be seen that the inverse relationship between amplitude and frequency observed during variations in C_r is approximately linear for small values of L (encompassing the range used in all simulations), but that this linearity breaks down for high values of L. In contrast, increases in L result in the gradual suppression of oscillatory activity, with minimal effects on oscillation frequency (at least for the range of values used in the simulations). The effect of variations of x_r (also illustrated in Fig. 3 *D*) demonstrates an inverse linear relationship between amplitude and frequency analogous to that observed for variations of C_r.

Nullcline analysis was also used to define the role of the RyR-activation Hill coefficient p_r and the Ca^{2+}-release Hill coefficient m_r in the genesis of oscillatory behavior. Decreases in p_r translated the intersection of the x and y nullclines downward, reducing the size of the associated limit cycle and its period and amplitude, until oscillatory behavior ceased when p_r fell below ~3 (Fig. 4 *A*). By contrast, the position of the nullcline intersection was relatively insensitive to changes in m_r, so that oscillatory activity was sustained at low values of this parameter (Fig. 4 *B*). However, high values of m_r resulted in rapid saturation of the Ca^{2+}-release mechanism and less complete emptying of the SR store, thus causing an elevation of the nullclines, i.e., increased $[Ca^{2+}]_{SR}$ for a given level of $[Ca^{2+}]_i$. This was associated with a reduction in oscillation amplitude and a decrease in the slow refilling period necessary to replenish stores, so that oscillation frequency was increased.

$InsP_3R$-mediated CICR

The kinetics of $InsP_3R$-mediated Ca^{2+} release was modeled with a dual Hill sigmoidal. At $[Ca^{2+}]_i$ levels <1 μM, the configuration of the x and y nullclines was closely similar to that of the RyR channel. Indeed, in the absence of complicating RyR activity (i.e., C_r set to zero), simulations

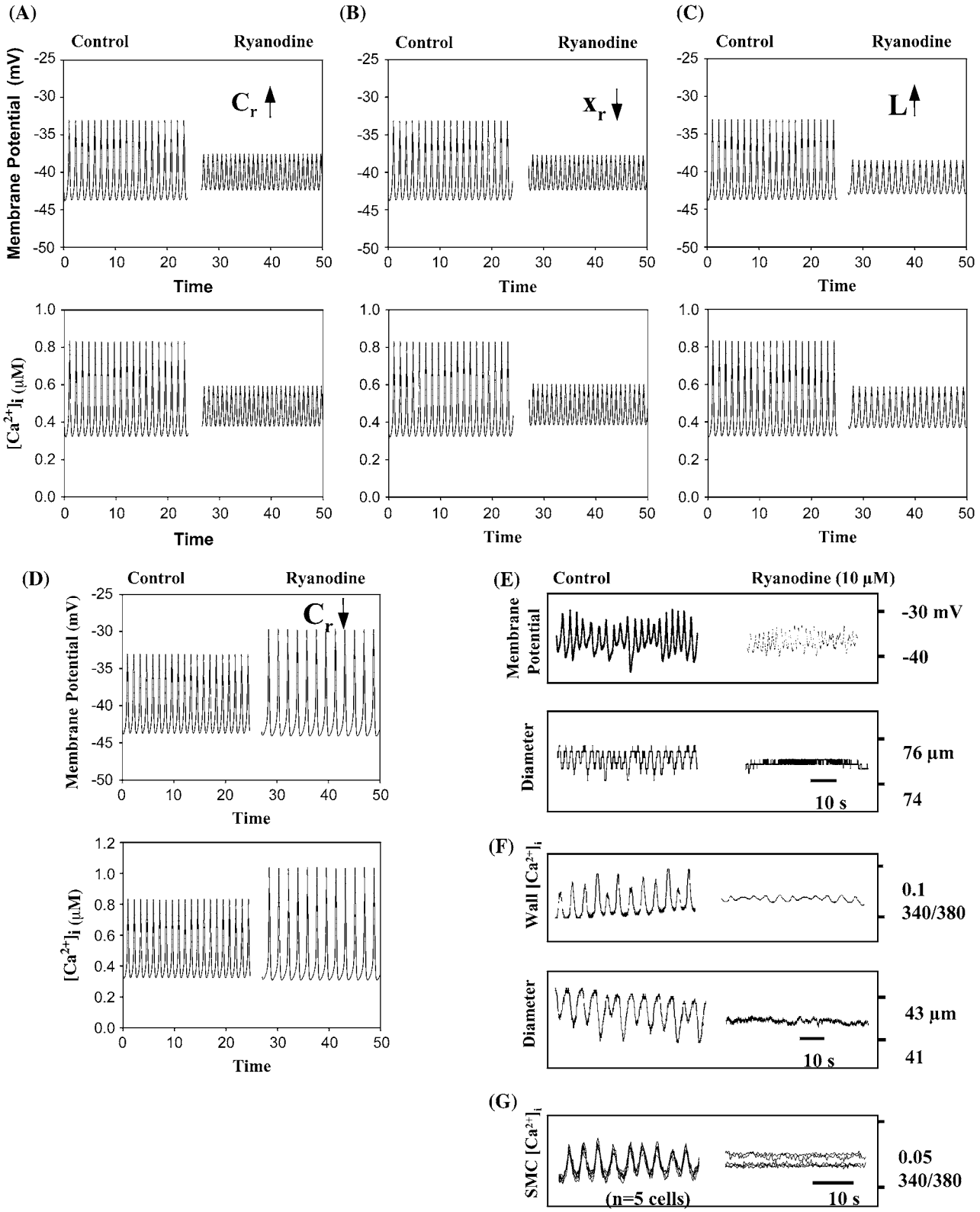

FIGURE 2 Four approaches simulating the reported actions of ryanodine by changing coefficients in Eqs. 1 and 2. (*A*) Increases in C_r from 1250 to 3250. (*B*) Decreases in the Ca^{2+} sensitivity coefficient x_c from 0.9 to 0.6. (*C*) Increases in L from 0.025 to 0.15. (*D*) Reductions in C_r from 1250 to 500. (*E–G*) Experimentally, ryanodine increased oscillatory frequency in association with a reduction in the amplitude of oscillations in diameter, membrane potential, global wall $[Ca^{2+}]$, and $[Ca^{2+}]$ in individual smooth muscle cells (SMC), but had little effect on their average values.

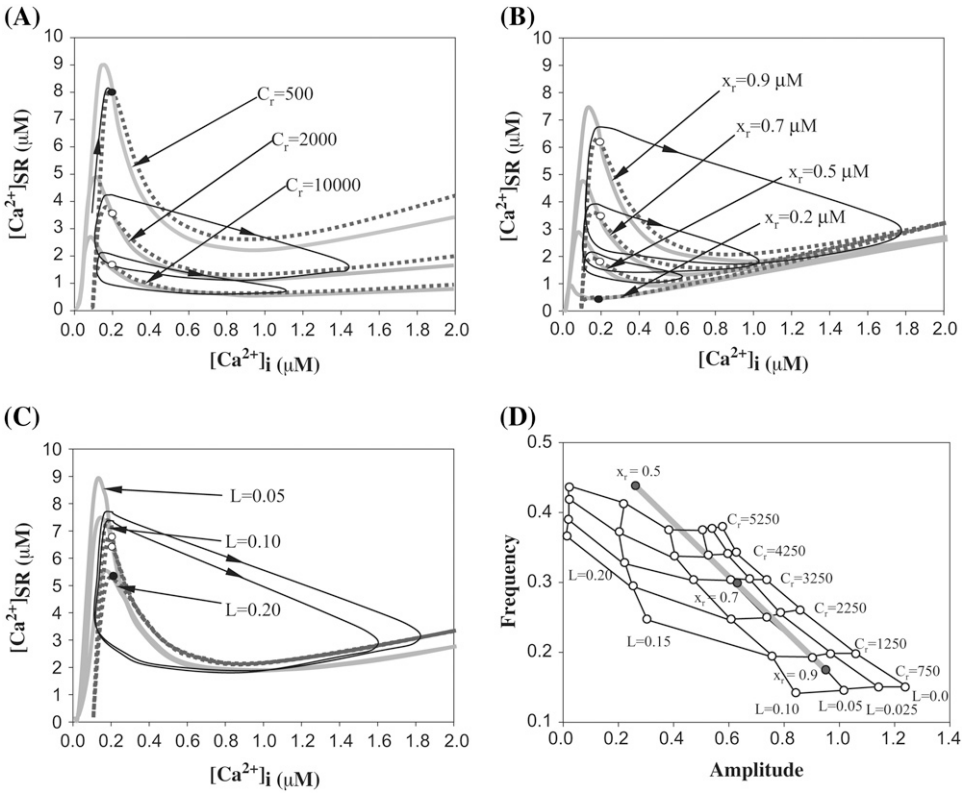

FIGURE 3 Nullcline analysis of the putative actions of ryanodine. (*A–C*) Pairs of nullclines and corresponding limit cycles for changes in parameters C_r, x_c, and L. The intersection of the x (*dashed line*) and y (*solid line*) nullclines determines the equilibrium points indicated by an open circle when unstable (i.e., oscillatory) and a solid circle when stable (nonoscillatory). In each case, progressive decreases in the coefficient under investigation ultimately suppressed oscillatory behavior. (*D*) Effects of these interventions on oscillation frequency and amplitude.

demonstrated that increases in the coefficient C_i to scale the flux of Ca^{2+} ions via the $InsP_3R$ channel or decreases in the coefficient x_i to enhance the Ca^{2+} sensitivity of the activating component of the biphasic open probability curve each reduced the size of the limit cycle and ultimately stopped oscillatory activity (Fig. 5, *A* and *B*). Compared to the RyR, the position of the nullclines relative to the y axis were elevated by the inactivating component of the $InsP_3R$ dynamics at $[Ca^{2+}]_i$ levels >1 μM, since $InsP_3R$ closure will curtail Ca^{2+} release above this level. Consequently, decreases in the inactivating coefficient h_i of the dual $InsP_3R$ Hill sigmoidal, which result in a leftward shift in the peak of the open probability curve of the $InsP_3R$ channel (Fig. 1), reduced the size of the limit cycle by progressively abbreviating the Ca^{2+}-release phase of the oscillatory mechanism (Fig. 5 *C*).

As in the case of the RyR dynamics, oscillations were observed only when the activating Hill slope p_i was above ~3 and the Hill exponent for Ca^{2+} release m_i influenced the size of the underlying limit cycle but did not determine the existence of oscillations (Fig. 6 *A* and *B*). The overall dynamics of the system was largely insensitive to changes in the secondary inactivating Hill slope q_i (Fig. 6 *C*).

Interactions between the RyR and $InsP_3R$

A value of C_i was selected so that the system was in a nonoscillatory regime and the value of C_r progressively increased, with the activation Hill coefficients of both channels taken as 4. This strategy allowed the emergence of oscillatory behavior, which ultimately ceased when the intersection of the x and y nullclines regained stability. As the

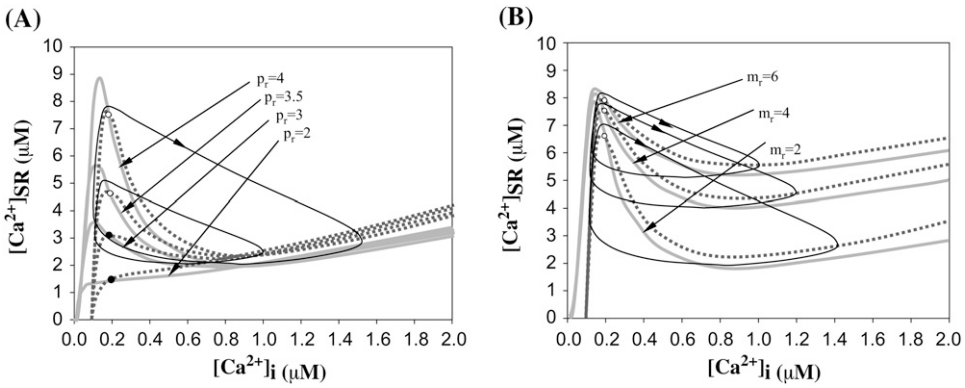

FIGURE 4 Effects of changes in the RyR Hill coefficients p_r and m_r. (*A*) Graded reductions in the activation coefficient p_r from 4 to 2 reduced the size of the limit cycle until oscillatory behavior ceased. (*B*) Reductions in the Ca^{2+} release coefficient m_r progressively increased the size of the limit cycle but did not stop oscillations. Dashed and solid lines denote the x and y nullclines; open and solid circles denote unstable and stable equilibrium points.

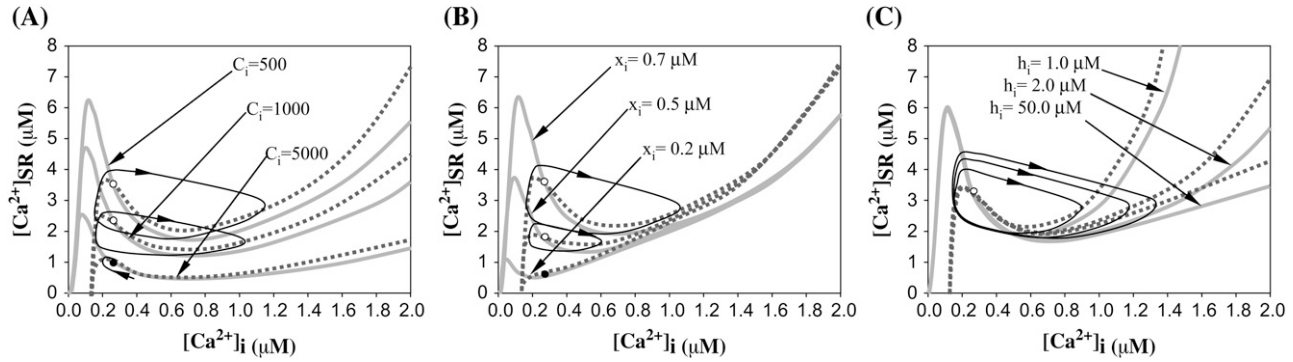

FIGURE 5 Nullcline analysis of the dynamics of $InsP_3R$-mediated CICR. (*A–C*) Pairs of nullclines and corresponding limit cycles for different values of the open probability coefficient C_i, activation sensitivity x_i and inactivation half-point h_i. Dashed and continuous lines denote the x and y nullclines; open and solid circles denote unstable and stable equilibrium points.

contribution of the RyR to the dynamics of the system was increased, the configuration of the nullclines progressively diverged from that associated with the $InsP_3R$ at $[Ca^{2+}]_i$ levels >1 μM, i.e., it changed from convex-up to flat. The overall effect was to translate the limit cycle downward as levels of $[Ca^{2+}]_{SR}$ decreased, but in contrast to the situation for the RyR alone, this translation was associated with a selective reduction in the store refilling phase of the limit cycle so that the amplitude of $[Ca^{2+}]_i$ oscillations remained effectively constant as their frequency increased (Fig. 7 *A*).

An analogous simulation was performed with a value of C_r selected such that the system did not exhibit oscillations and the value of C_i progressively increased. Again this resulted in the emergence of an unstable nullcline intersection point that eventually regained stability. In this scenario, the limit cycle was translated downward but became globally smaller, with reduced amplitude and period, until it disappeared (Fig. 7 *B*). The nullcline analysis shown in Fig. 7, *A* and *B*, was performed with z held at –40 mV; attractors generated by simulations in which membrane potential z contributed to the dynamics as an independent variable (i.e., by the full three-dimensional model of Eqs. 1–3) illustrate similar general behavior (Fig. 7, *C* and *D*).

The mathematical structure of the model necessarily implies that CICR mediated either by the RyR and/or the $InsP_3R$ will not be a principal determinant of mean $[Ca^{2+}]_i$. This can be appreciated by equating dx/dt and dy/dt to zero to define the unstable equilibrium point around which intracellular Ca^{2+} oscillations develop. Addition of Eqs. 1 and 2 then gives

$$A - G_{Ca}\frac{z - z_{Ca_1}}{1 + e^{-(z - z_{Ca_2})/R_{Ca}}} + G_{Na/Ca}\frac{x^*}{x^* + x_{Na/Ca}}(z - z_{Na/Ca}) - Dx^{*k}\left(1 + \frac{z - z_d}{R_d}\right) = 0. \quad (4)$$

It follows that x^*, the equilibrium value of $[Ca^{2+}]_i$, is independent of C_r, C_i, B, and L and also the Hill coefficients of the RyR and $InsP_3R$ sigmoidals. This idea gains support from the experimental finding that ryanodine did not significantly affect mean values of wall $[Ca^{2+}]_i$ or $[Ca^{2+}]_i$ in individual smooth muscle cells in the rat basilar artery (Fig. 2). It should be noted, however, that x^* provides only a guide to the mean value of $[Ca^{2+}]_i$ when the dynamics of the system support the existence of a limit cycle, since x^* will be

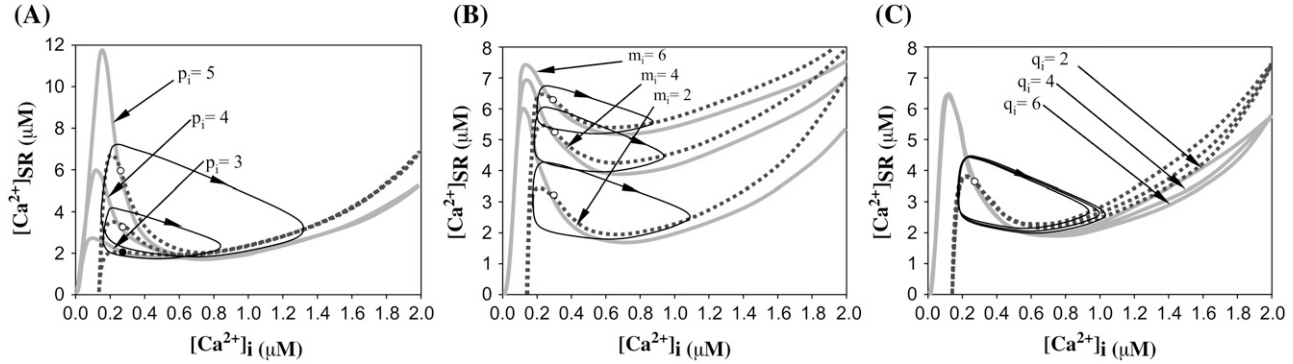

FIGURE 6 Nullcline analysis for the activating and inactivating $InsP_3R$ Hill coefficients. Plots are shown for (*A*) the activation coefficient p_i,, (*B*) the store release coefficient m_i, and (*C*) the inactivation coefficient q_i. Dashed and solid lines denote the x and y nullclines; open and solid circles denote unstable and stable equilibrium points.

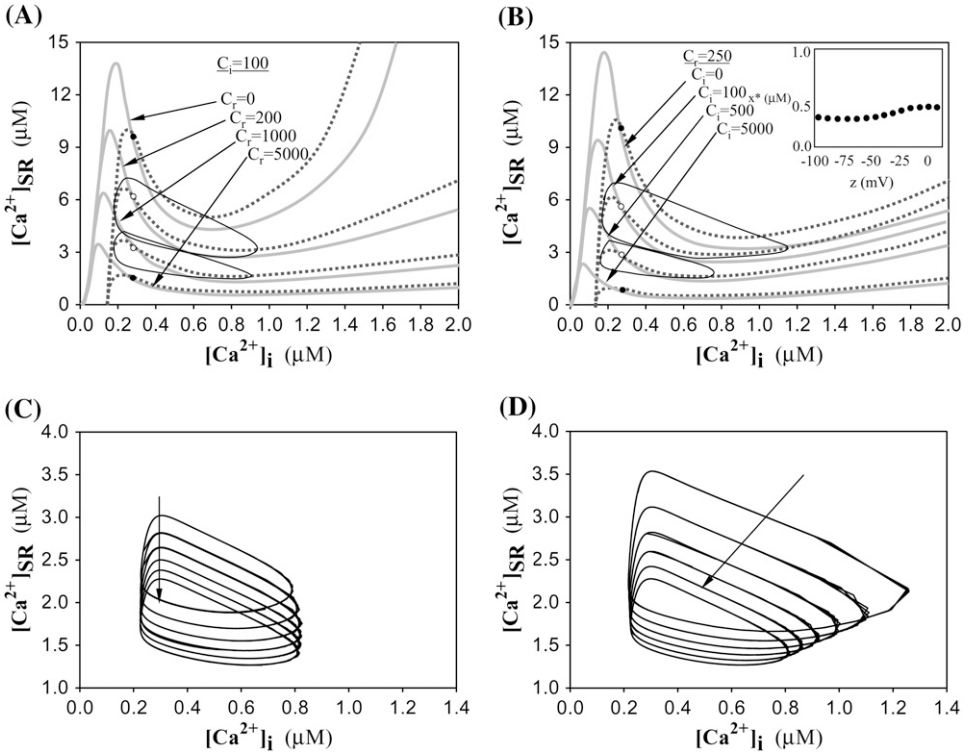

FIGURE 7 Analysis of combined RyR- and $InsP_3R$-mediated CICR. (*A*) Progressive activation of Ca^{2+} release by ryanodine (simulated as an increase in C_r) in the presence of fixed $InsP_3$-mediated CICR (constant C_i) can initiate or suppress oscillatory activity. (*B*) Similar analysis for progressive increases in coefficient C_i for fixed C_r. (*C* and *D*) Two-dimensional projections of the full three-dimensional attractor of the dynamics. Increases in coefficients C_r and C_i translate the attractors in the direction of the arrows. The inset in *B* illustrates the relationship between the equilibrium values $[Ca^{2+}]_i$ (x^*) and membrane potential (z^*) as a solution of Eq. 4. Dashed and solid lines denote the x and y nullclines; open and solid circles denote unstable and stable equilibrium points. Nullclines and limit cycles were obtained with z held at −40 mV; attractors were generated from trajectories where z was a free variable.

dependent on cell membrane potential. Indeed, as noted above, all nullcline analysis was performed with a constant z to eliminate the effect of the membrane potential on the dynamics of the system and maintain a strictly two-dimensional oscillatory regime that allows clear visualization of the effects of specific parameter changes. To evaluate the consequences of this simplification, the dependence of the equilibrium values x^* on z was quantified by using Eq. 4 to plot x^* as a function of z (Fig. 7 *B*, *inset*). The plot demonstrates that for a broad range of z values within the physiological range (−70 to −20 mV) there was only a small impact on x^* (<0.1 μM).

Role of membrane transport systems

In all simulations designed to investigate the contribution of transmembrane ion fluxes to vasomotion, C_r was assigned the same initial default value with the coefficient C_i set to zero. Although this computational simplification implies that $InsP_3R$ activity does not participate in intracellular Ca^{2+} dynamics, it should be appreciated from the above analysis that general conclusions concerning the role of different membrane transport systems will not differ whether CICR is modeled mathematically as an RyR- or $InsP_3R$-dependent process within the physiological operating range for $[Ca^{2+}]_i$.

Calcium influx via NSCCs

The PLC inhibitor U73122 will attenuate influx of extracellular Ca^{2+} ions into the cytosol via NSCCs by depressing the formation of DAG, and the contribution of this mechanism to vasomotion was investigated by reducing the coefficient A in Eq. 1. Such simulations resulted in membrane hyperpolarization, a reduction in mean $[Ca^{2+}]_i$, and complete suppression of oscillatory activity (Fig. 8 *A*). Experimentally, closely analogous effects on membrane potential and $[Ca^{2+}]_i$ were observed after administration of 10 μM U73122, which caused dilatation and abolished rhythmic activity in rat isolated basilar arteries (Fig. 8, *B–D*). Taken together, these theoretical and experimental findings demonstrate the crucial role of Ca^{2+} influx in the maintenance of rhythmic activity and suggest that the pharmacological action of U73122 is dominated by its effects on DAG formation rather than $InsP_3$ synthesis.

Calcium influx via VOCCs

The action of the VOCC blocker nifedipine was simulated by reducing the coefficient G_{Ca} in Eqs. 1 and 3 (Fig. 9). In general, this strategy tended to cause slight membrane hyperpolarization and a decrease in $[Ca^{2+}]_i$, although the effects of reductions in G_{Ca} on the amplitude of oscillatory activity depended on the magnitude of the flux of Ca^{2+} ions into the cytosol via NSCCs relative to that entering via VOCCs. When DAG-mediated Ca^{2+} influx via NSCCs (coefficient A in Eq. 1) was high, oscillations persisted even when blockade of VOCCs was complete (Fig. 9 *A*). By contrast, when this Ca^{2+} influx via NSCCs was less dominant (i.e., A was low), suppression of the inward Ca^{2+} current via VOCCs resulted in complete loss of oscillatory activity (Fig. 9 *B*). Experimentally, 1 μM nifedipine suppressed oscillations in membrane potential, wall calcium, and vessel

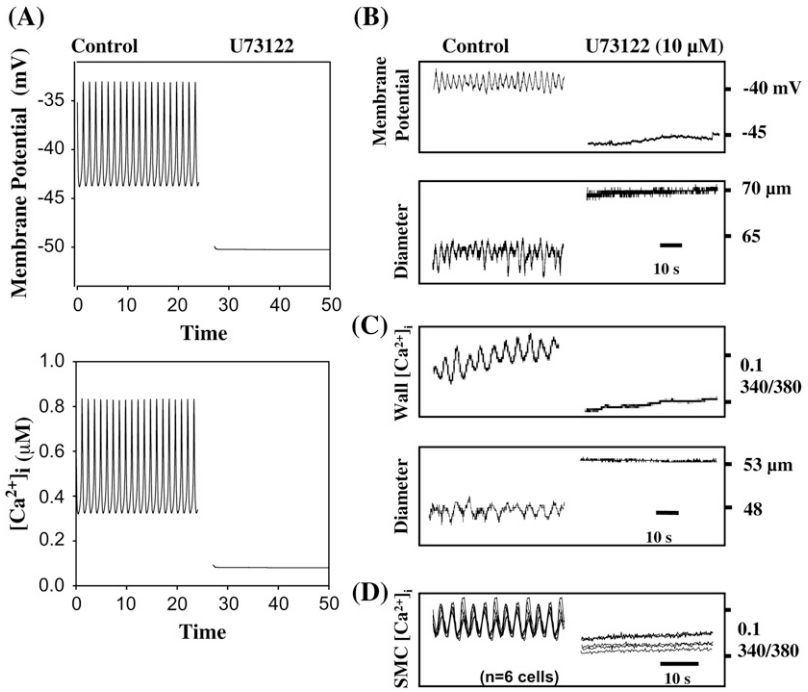

FIGURE 8 (*A*) Reductions in term *A* of Eq. 1 were used to simulate the action of U73122 (from $A = 2.3$ to $A = 0.0$). (*B*) Experimentally, 10 μM U73122 caused membrane hyperpolarization, dilatation and loss of rhythmic activity. (*C* and *D*) 10 μM U73122 also inhibited oscillations in global wall $[Ca^{2+}]$ and cytosolic $[Ca^{2+}]_i$ in individual smooth muscle cells.

diameter, as predicted by the simulations (Fig. 9, *C–E*). These findings further emphasize the role of extracellular Ca^{2+} influx in the genesis of vasomotion.

Bifurcation analysis of Ca^{2+} influx

To clarify the dynamical connection between Ca^{2+} fluxes via VOCCs and NSCCs, a bifurcation diagram for $[Ca^{2+}]_i$ oscillations was constructed for variations in the control parameters G_{Ca} and A (Fig. 10 *A*). Decreases in G_{Ca} first produced a Hopf bifurcation into an oscillatory regime, but oscillations were subsequently suppressed via the reverse Hopf scenario, when Ca^{2+} uptake via VOCCs was further reduced. For large values of A, the oscillatory regime was maintained throughout the physiological range of G_{Ca} (i.e., $G_{Ca} \geq 0$). Ca^{2+} flux via NSCCs (i.e., coefficient A) therefore represents a control parameter that determines whether oscillatory activity will be abolished or sustained during complete blockade of VOCCs. The transition between these cases (corresponding to low and high NSCC fluxes) is also presented as time series in Fig. 10 *B*.

The interplay between extracellular Ca^{2+} influx via NSCCs and VOCCs and RyR-mediated intracellular Ca^{2+} release was also investigated by nullcline analysis of the effects of variations in the coefficients A, G_{Ca}, and C_r. This analysis illustrates how low and high levels of influx via either channel generally lead to the loss of oscillatory activity, although there is also a crucial dependence on C_r (Fig. 11, *A* and *B*).

Effects of charybdotoxin

The effects of the Ca^{2+}-activated K^+ channel (K_{Ca}) inhibitor charybdotoxin were simulated by reducing the coefficient G_K in Eq. 3 (Fig. 12 *A*). This strategy induced membrane depolarization, elevated mean $[Ca^{2+}]_i$, and reduced the amplitude of oscillations in these variables in association with an increase in their frequency (Fig. 12 *A*). Experimentally, 60 nM charybdotoxin depolarized the smooth muscle of the rat basilar artery and increased both wall and cell $[Ca^{2+}]_i$ in association with constriction (Fig. 12, *B–D*). In the example shown, the reduction in amplitude (~80%) and the increase in frequency (~50%) were of the same order of magnitude as the simulations illustrated in Fig. 12 *A*.

Role of chloride channels

The role of chloride channels was probed with two alternative strategies: 1), substitution of extracellular chloride ions to enhance Cl^- extrusion; and 2), direct pharmacological blockade of Cl^- channels.

1. Stepwise changes in $[Cl^-]_o$ were modeled as a discrete shift in the operating Cl^- reversal potential after the introduction of a 17-mV Δz_{Cl} step in the voltage dependence of the Cl^- channel in Eq. 3, i.e., $-G_{Cl}(x/(x + x_{Cl}))(z - (z_{Cl} + \Delta z_{Cl}))$. This approach resulted in a membrane depolarization of ~10 mV that was accompanied by an increase in $[Ca^{2+}]_i$ and loss of rhythmic activity (Fig. 13 *A*). Experimentally, the effects of chloride substitution with 120 mM sodium isethionate closely matched these simulations, showing a marked depolarization and increase in $[Ca^{2+}]_i$ in association with sustained constriction (Fig. 13, *B–D*).
2. Pharmacological interventions with the Cl^- channel blocker niflumic acid were simulated by reducing the coefficient G_{Cl} in Eq. 3. This suppressed oscillatory

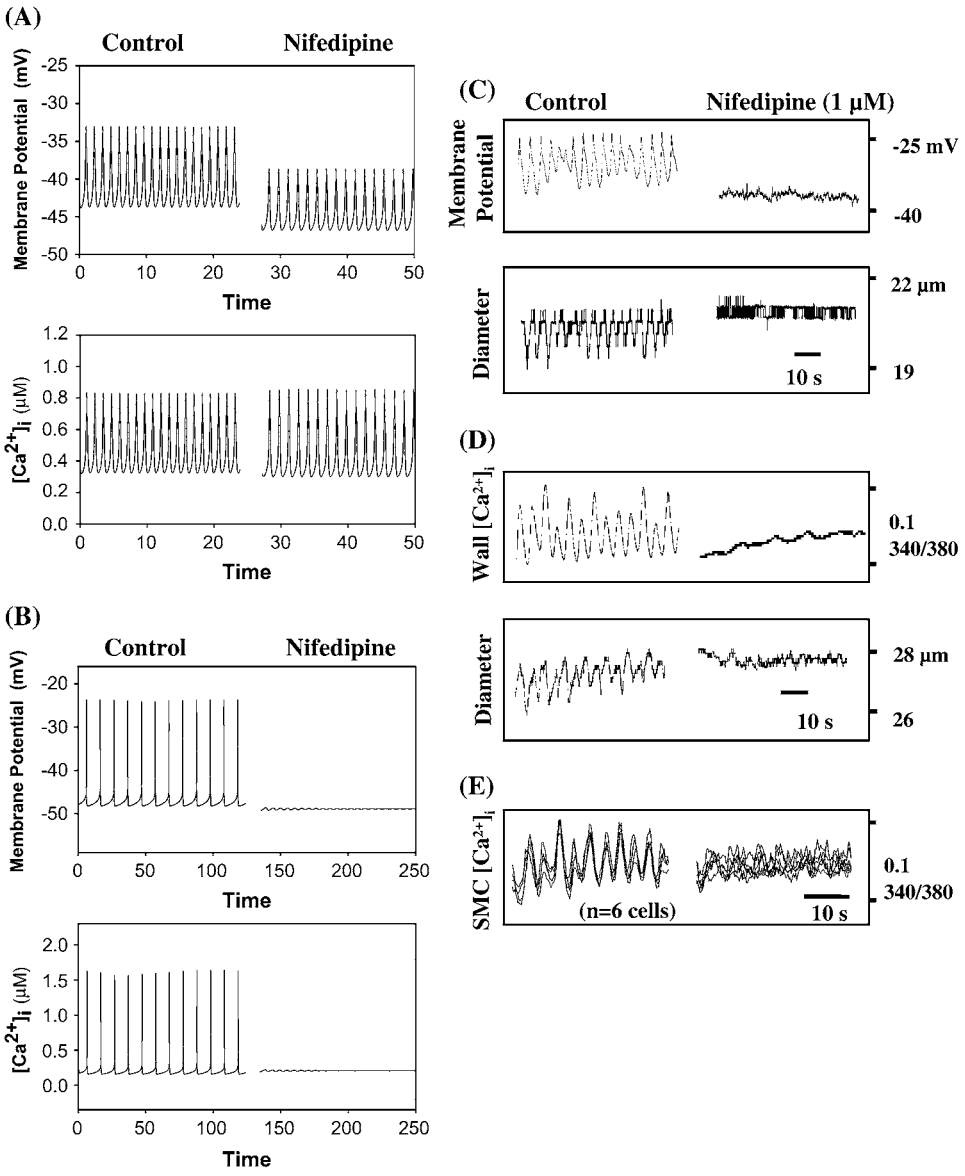

FIGURE 9 (*A* and *B*) Reductions in the coefficient G_{Ca} of the VOCC term in Eqs. 1 and 3 from 12 to 0 were used to simulate the action of nifedipine. When coefficient *A* was relatively large (2.3 (*A*)) blockade of VOCCs did not suppress oscillatory activity, whereas for small values of *A* (0.7 (*B*)) oscillations were abolished. (*C–E*) Experimentally, 1 μM nifedipine effectively abolished vasomotion with oscillations in wall $[Ca^{2+}]$ and in individual smooth muscle cells being markedly reduced in amplitude.

activity completely in association with membrane hyperpolarization (Fig. 13 *E*). Experimental findings with 50 μM niflumic acid closely matched these theoretical predictions (Fig. 13, *F–H*).

Integrated behavior of membrane transport systems

The contributions of K^+ efflux, Na^+/Ca^{2+} exchange, Cl^- channels, and Ca^{2+} influx through VOCCs to dynamic changes in membrane potential (dz/dt) are plotted as a function of membrane potential in Fig. 14 *A*, with the ordinate showing the individual and summed effects of these transport systems. The composite dz/dt curve intersects the horizontal axis at three points, which represent possible steady states where oscillations in membrane potential and $[Ca^{2+}]_i$ may be abolished, with the central equilibrium point (P2) unstable but the outer points (P1 and P3) stable. Families of dz/dt plots were calculated from Eq. 3 to gain insight into the actions of the pharmacological probes as follows:

1. Each of the plots presented in Fig. 14 *B* corresponds to a single value of $[Ca^{2+}]_i$ between 0.1 and 0.9 μM, and it can be seen that reductions in $[Ca^{2+}]_i$ translate the P1 stable equilibrium to the left and thereby promote hyperpolarization. Although the effects of $[Ca^{2+}]_i$ on dz/dt are viewed at constant values of $[Ca^{2+}]_i$, and therefore do not reproduce the dynamics of Eqs. 1–3 under oscillatory conditions, such plots provide insight into the behavior of the system after administration of the PLC inhibitor U73122, which will reduce time-averaged

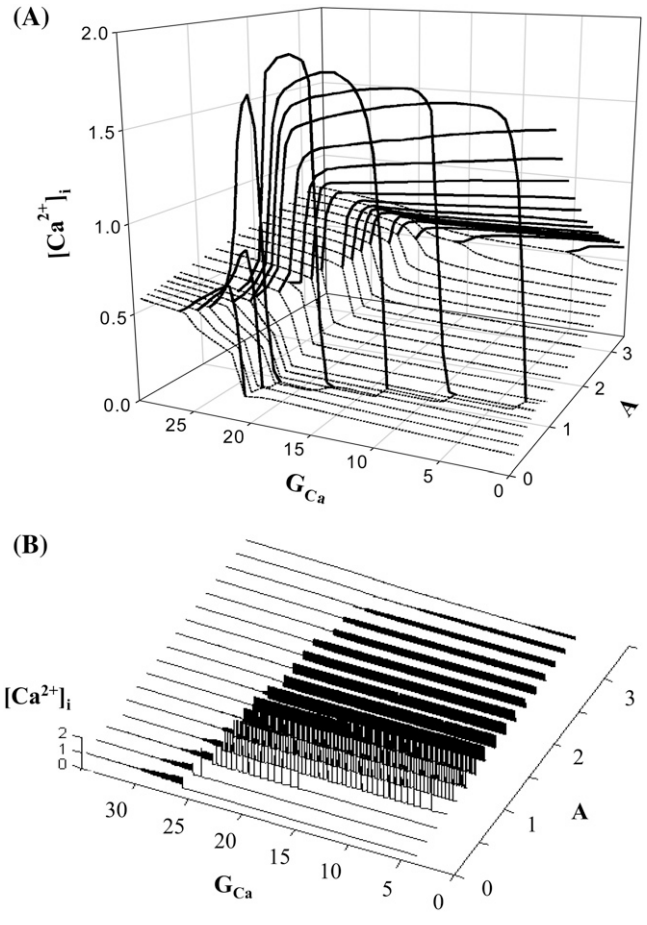

FIGURE 10 Bifurcation analysis of $[Ca^{2+}]_i$ oscillations constructed by varying the parameters G_{Ca} (VOCCs) and A (NSCCs). (*A*) G_{Ca} was varied from 30.0 to 0.0, whereas A was varied from 0.1 to 3.3. Decreases in G_{Ca} demonstrate the occurrence of a Hopf bifurcation followed by a reverse Hopf bifurcation when G_{Ca} is further decreased. The reverse Hopf bifurcation occurs outside the physiological range (i.e., $G_{Ca} < 0$) for large A values, thus indicating that oscillatory activity may either be abolished (low A) or sustained (high A) after blockade of VOCCs. (*B*) Corresponding time series illustrating the oscillatory and nonoscillatory domains in G_{Ca}-A parameter space.

$[Ca^{2+}]_i$ by suppressing the net influx of Ca^{2+} ions via NSCCs into the cytosol.

2. Reductions in G_{Ca} to simulate blockade of VOCCs result in a depression of the bell-shaped maximum in dz/dt at membrane potentials close to 0 mV with a leftward shift in the P1 stable equilibrium and hyperpolarization (Fig. 14 *C*). Displacement is more marked for high-$[Ca^{2+}]_i$ (depolarized) than for low-$[Ca^{2+}]_i$ (hyperpolarized) states where the effect of Ca^{2+} currents through VOCCs is minimal. This distinction suggests that the effects of nifedipine will be most pronounced in the depolarized range around 0 mV rather than when the membrane is hyperpolarized.
3. Reductions in G_K to simulate blockade of K_{Ca} channels by charybdotoxin deflect the dz/dt curves upward by effectively rotating them around the K_{Ca} reversal potential at ~ -95 mV (Fig. 14 *D*). Note that for low values of G_K crossings of the horizontal axis at P1 and P2 may disappear, leaving only the depolarized stable point P3. This suggests that under certain circumstances trajectories will jump to an equilibrium where oscillations are not observed.
4. The two distinct pharmacological interventions used to probe the contribution of Cl^- channels to vasomotion can be understood in an analogous fashion. Substitution of extracellular Cl^- by sodium isethionate will enhance extrusion of this ion from the intracellular compartment and was modeled by a 17-mV stepwise increase in the reversal potential for chloride ions, Δz_{Cl}. This approach resulted in a direct upward translation of the dz/dt curves and was associated with a membrane depolarization Δz of $\sim$10 mV (Fig. 14 *E*). Simulations (not shown) confirmed that the scaling between Δz_{Cl} and Δz is determined largely by coefficient G_{Cl} and is essentially independent of other model parameters, as suggested by inspection of Eqs. 3 and 4. Cl^- substitution will thus result in a stepwise membrane depolarization of effectively constant magnitude (e.g., Fig. 13 *A*). By contrast, blockade of Cl^- channels by niflumic acid rotates the dz/dt curves anticlockwise around the Cl^- reversal potential. This causes hyperpolarization below the Cl^- reversal potential (as will normally be the case in the physiological situation), but depolarization above this potential (Fig. 14 *F*).

By employing the three-variable model, it is possible to visualize the dynamical attractor of the system as a three-dimensional plot of $[Ca^{2+}]_i$ versus $[Ca^{2+}]_{SR}$ versus membrane potential. Such an attractor and its evolution in time after stepwise changes in drug concentrations are presented in Fig. 15 for each individual pharmacological intervention. The shape of the attractor, shown in Fig. 15 *A*, for stepwise changes in the coefficients A, C_r, and G_{Ca} suggests a general trend from high $[Ca^{2+}]_i$ (low $[Ca^{2+}]_{SR}$), where no oscillatory behavior can occur, to a regime of sustained large amplitude oscillations that are ultimately suppressed at low $[Ca^{2+}]_i$ (high $[Ca^{2+}]_{SR}$), an overall scenario that can describe the action of U73122, ryanodine, and nifedipine (Fig. 15, *A–C*). Pharmacological agents that indirectly affect $[Ca^{2+}]_i$ by causing changes in membrane potential, such as charybdotoxin, isethionate, and niflumic acid (Fig. 15, *D–F*), induce a different effect as they translate the attractor parallel to the z axis in association with ultimate suppression of oscillatory activity. Antagonism between K^+ and Cl^- channels becomes apparent by noting the opposite trends in Fig. 15, *D* and *F*, in which blockade of K^+ channels by charybdotoxin promotes depolarization, and blockade of Cl^- channels by niflumic acid promotes hyperpolarization.

It should be noted that in all simulations presented in previous sections neither K^+ nor Cl^- channels were assumed to be activated by Ca^{2+}, i.e., $\beta = 0$ and $x_{Cl} = 0$, so that their contribution to membrane potential in Eq. 3 simplifies to $G_K(z - z_K)$ and $G_{Cl}(z - z_{Cl})$. Simulations of the action of charybdotoxin with $\beta = 0$ and 0.1 (i.e., in the absence and

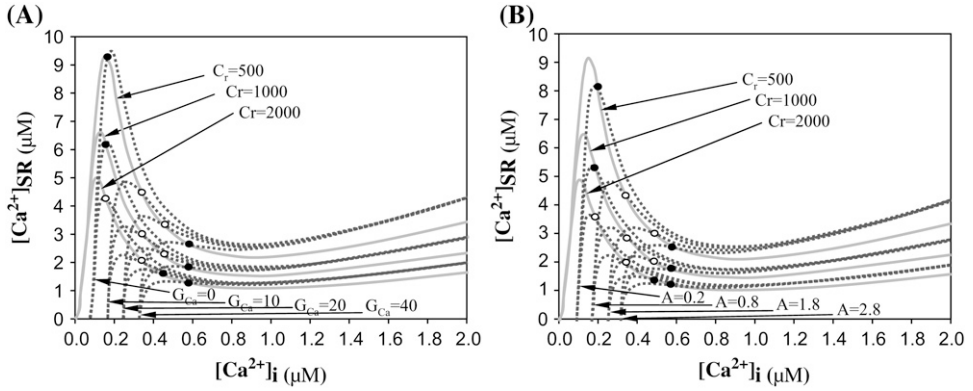

FIGURE 11 Nullcline analysis illustrating the stability characteristics of the system under the variation of (*A*) parameters C_r and G_{Ca} (with $A = 0.5$), and (*B*) parameters C_r and A (with $G_{Ca} = 12$). Dashed and solid lines denote the x and y nullclines; open and solid circles denote unstable and stable equilibrium points.

presence of Ca^{2+} dependence) showed that equal reductions in the coefficient G_K suppressed oscillatory activity more quickly for $\beta = 0.1$ (Fig. 16 *A*). The effects of Ca^{2+} dependence of the Cl^- channels were investigated by comparing the action of 1), isethionate with $x_{Cl} = 0$ and 0.1; and 2), niflumic acid with $x_{Cl} = 0$ and 0.15. Isethionate suppressed oscillatory activity more slowly when Ca^{2+} sensitivity of Cl^- channels was incorporated in the model (Fig. 16 *B*), whereas niflumic acid suppressed oscillations more rapidly (Fig. 16 *C*).

DISCUSSION

The aim of this study was to develop and validate a minimal mathematical model of the interacting ion transport systems that regulate smooth-muscle tone and underpin vasomotion in the rat basilar artery. The model incorporates three nonlinear differential equations to describe the regulation of free cytosolic $[Ca^{2+}]$, $[Ca^{2+}]$ in intracellular stores, and smooth-muscle membrane potential and was formulated on the basis that the ''macroscopic'' rhythmic behavior of the arterial wall reflects ion movements occurring at the level of the single cell. Empirically, this assumption can be justified on the basis that the onset of vasomotion coincides with the synchronization of intracellular Ca^{2+} oscillations and intracellular waves in large populations of smooth muscle cells (7,9–11,13). To validate the approach, system parameters determining a range of ionic fluxes were varied to model pharmacological interventions, and these simulations compared with corresponding experimental measurements of smooth-muscle membrane potential, $[Ca^{2+}]_i$, and vascular caliber.

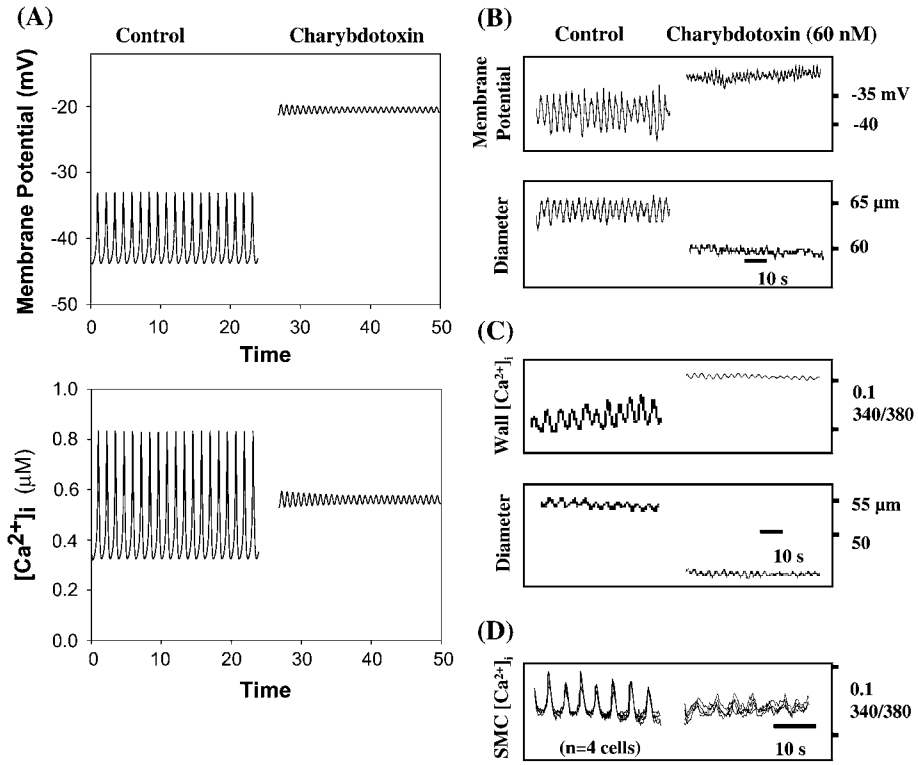

FIGURE 12 A reduction in the coefficient G_K of Eq. 3 was used to simulate the action of charybdotoxin. (*A*) Oscillatory activity was almost abolished when G_K was reduced from 43 to 28, in association with marked membrane depolarization and increased $[Ca^{2+}]_i$. (*B*) Experimentally, charybdotoxin (60 nM) markedly reduced the amplitude of contractile and electrical activity and caused membrane depolarization. The residual activity exhibited an increase in frequency. (*C* and *D*) Oscillations in wall Ca^{2+} and in individual smooth muscle cells were similarly increased in frequency with a rise in mean $[Ca^{2+}]$.

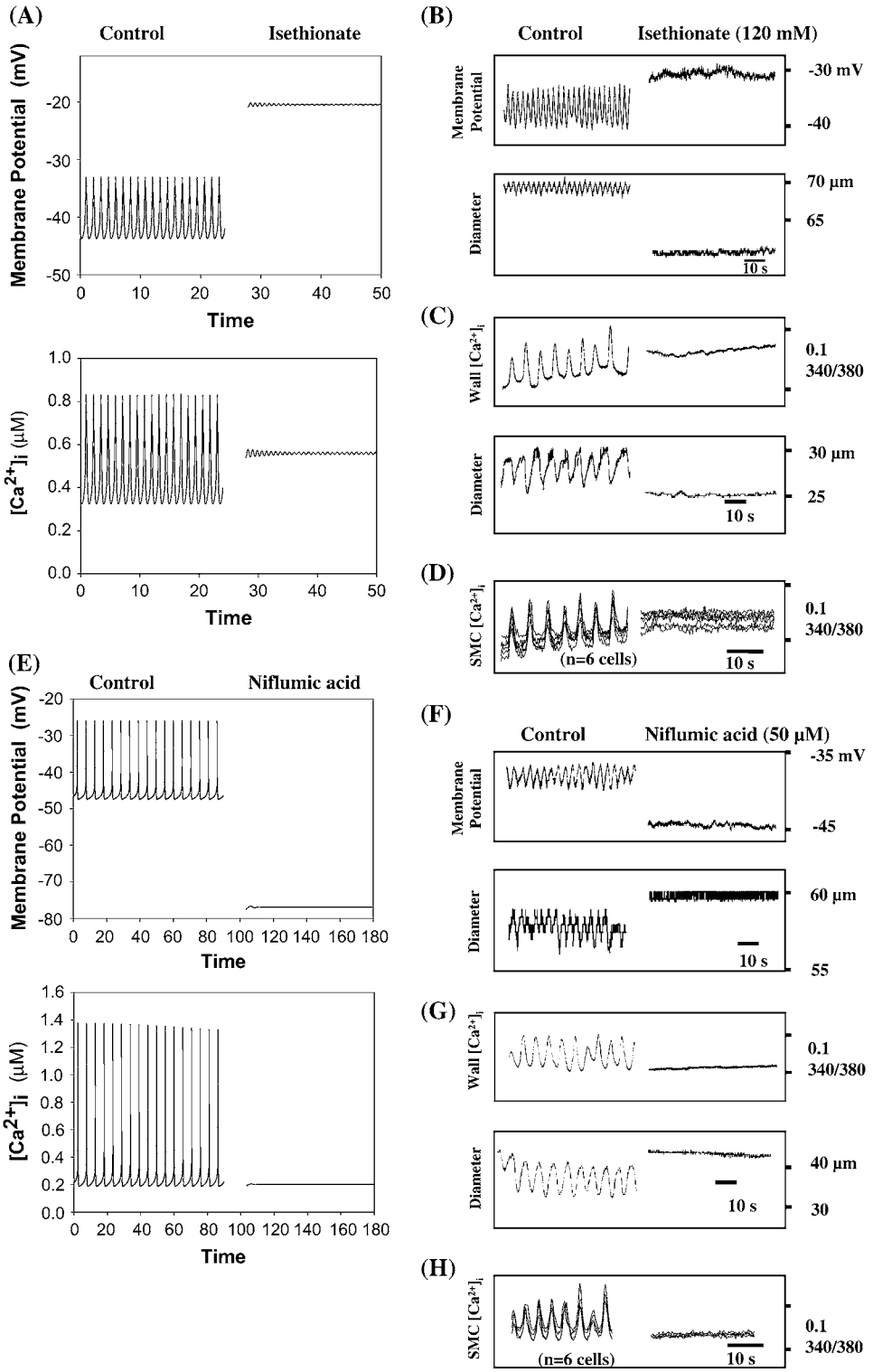

FIGURE 13 (*A*) Action of sodium isethionate simulated by introducing a stepwise change in the Cl^- channel reversal potential z_{Cl} by a Δz_{Cl} of 17 mV, which resulted in significant membrane depolarization, a slight rise in average $[Ca^{2+}]_I$, and suppression of oscillatory behavior. (*B–D*) Experimentally, chloride substitution with 120 mM sodium isethionate caused depolarization and abolished rhythmic contractile activity and Ca^{2+} oscillations and also caused a small increase in mean $[Ca^{2+}]_i$. (*E*) Simulation of the action of chloride channel blocker niflumic acid by reducing coefficient G_{Cl} from 65 to 0 (with $A = 1.0$) resulted in hyperpolarization and a reduction in $[Ca^{2+}]_i$. (*F–H*) Experimentally, niflumic acid resulted in hyperpolarization and a reduction in $[Ca^{2+}]_i$ with an associated loss of rhythmic activity.

Cytosolic Ca^{2+} cycling via the RyR and $InsP_3R$

In the rat cerebral artery, ryanodine suppressed oscillations in membrane potential and $[Ca^{2+}]_i$, consistent with studies in a range of rat and rabbit arteries that have previously demonstrated an essential role for stores expressing the RyR in the genesis of vasomotion, and in which ryanodine has been found to attenuate or abolish rhythmic mechanical activity and oscillations in smooth-muscle $[Ca^{2+}]$ and membrane potential (1,4,5,7,8,17,56). By contrast, in rat portal vein myocytes the regulation of $[Ca^{2+}]_i$ involves cooperativity between the RyR and the $InsP_3R$, with oscillatory activity

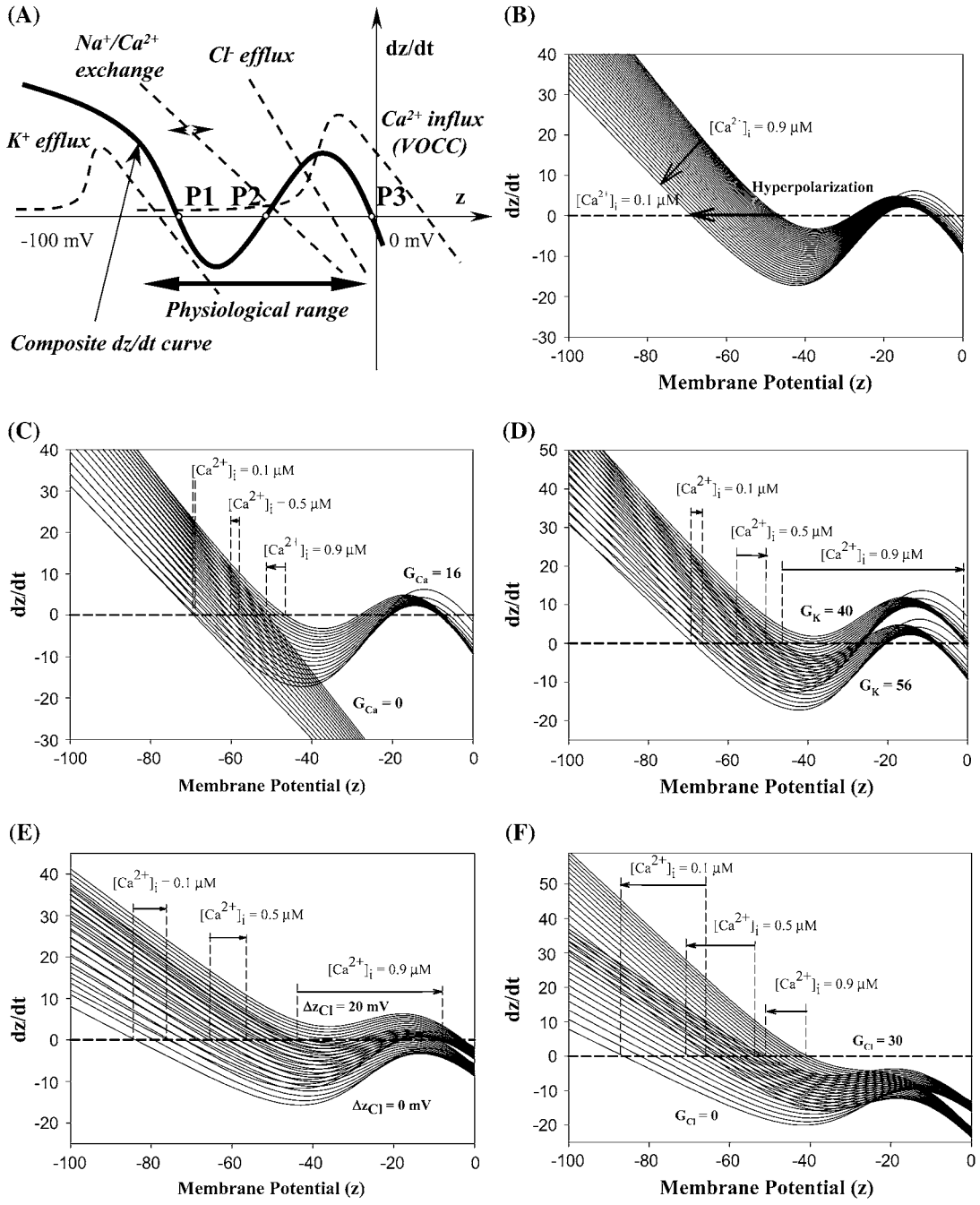

FIGURE 14 (*A*) Over the physiological range, individual components contributing to membrane potential include K^+ efflux, which promotes hyperpolarization, whereas Cl^- efflux and Ca^{2+} influx through VOCCs both promote depolarization. The role of Na^+/Ca^{2+} exchange is variable because of the Ca^{2+} dependence of the reversal potential of this exchange mechanism. A hypothetical composite *dz/dt* plot (see Eq. 3) shows that three possible steady states occur at points of intersection with the horizontal axis (P1 and P3, stable; P2, unstable). (*B*) Family of *dz/dt* plots encompassing the physiological range, with each plot corresponding to a distinct value of $[Ca^{2+}]_i$ at intervals of 0.05 μM, as indicated. The plots provide insight into the hyperpolarizing action of U73122 as this agent decreases $[Ca^{2+}]_i$. (*C*) The effects of nifedipine were modeled as a reduction of G_{Ca} to generate two families of *dz/dt* plots, each covering the range $[Ca^{2+}]_i$ = 0.1–0.9 μM. Theoretical effects of nifedipine on membrane potential are indicated by arrows at the same value of $[Ca^{2+}]_i$ and show that hyperpolarization is most marked in depolarized vessels when $[Ca^{2+}]_i$ is high. (*D*) Analogously, the depolarizing effects of charybdotoxin were modeled by reducing G_K to generate two families of plots encompassing different values of $[Ca^{2+}]_i$. The corresponding depolarizations are indicated by arrows. (*E* and *F*) A similar approach was used to understand the role of Cl^- channels after substitution by isethionate or administration of niflumic acid. These simulations respectively demonstrate depolarization and hyperpolarization.

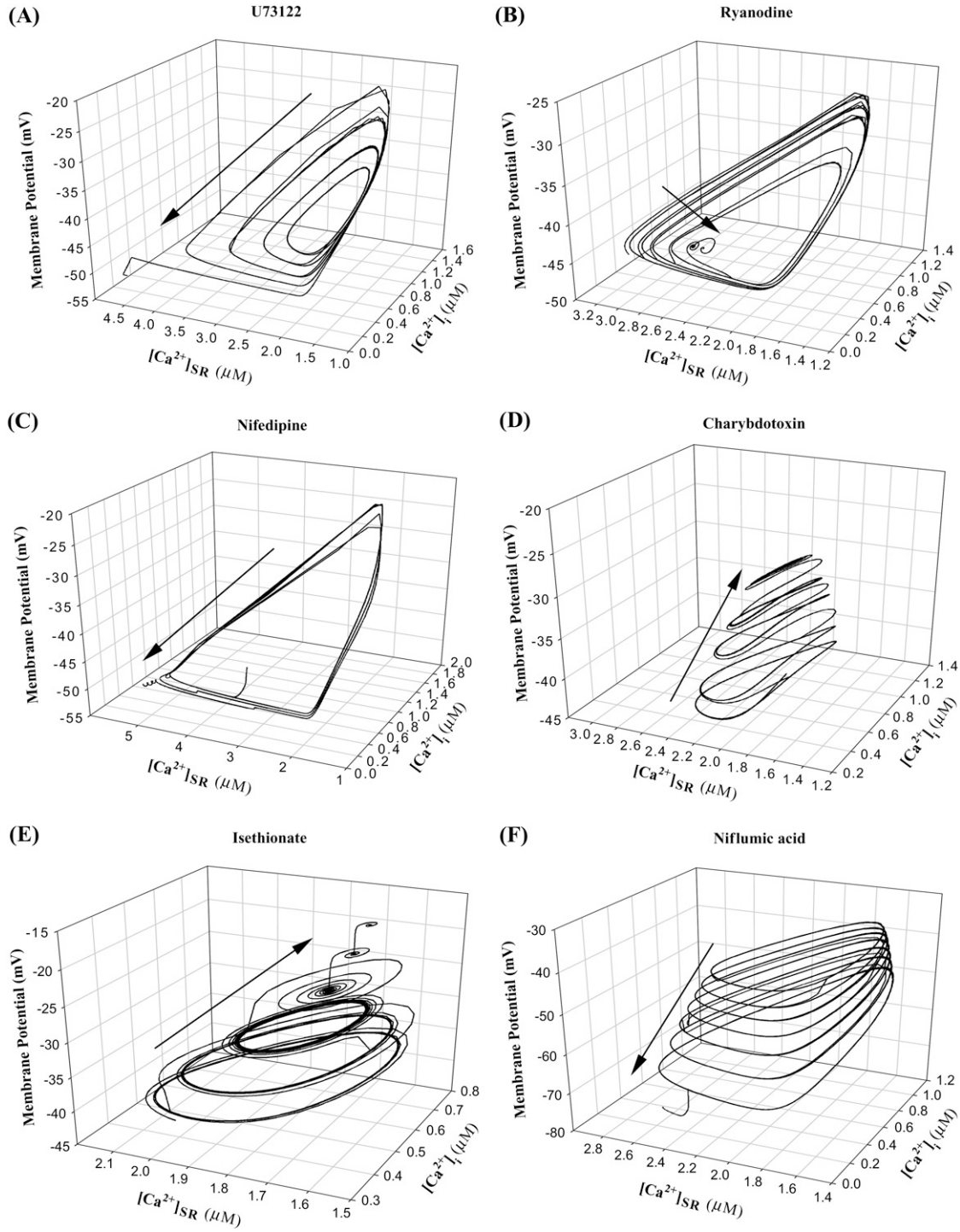

FIGURE 15 (*A*) U73122, simulated as stepwise reductions in term *A*, promotes membrane hyperpolarization and suppression of oscillatory activity. (*B*) Ryanodine, simulated as stepwise increases in coefficient *C*, is associated with a gradual reduction in oscillatory amplitude as $[Ca^{2+}]_{SR}$ is reduced and stores are gradually depleted. There is minimal effect on average $[Ca^{2+}]_i$ and membrane potential. (*C*) Nifedipine, modeled as stepwise decreases in coefficient G_{Ca}, causes a reduction in both $[Ca^{2+}]_i$ and membrane potential. (*D*) Charybdotoxin, simulated as decreases in coefficient G_K of Eq. 3, induces marked depolarization and an increase in $[Ca^{2+}]_i$. (*E*) Chloride substitution by isethionate, modeled as changes in z_{Cl}, produced marked membrane depolarization, associated with a small increase in mean $[Ca^{2+}]_i$ and ultimate suppression of oscillatory activity. (*F*) Chloride channel blocking by niflumic acid produced hyperpolarization and reduced $[Ca^{2+}]_i$. Arrows indicate the direction in which the attractor translates during intervention.

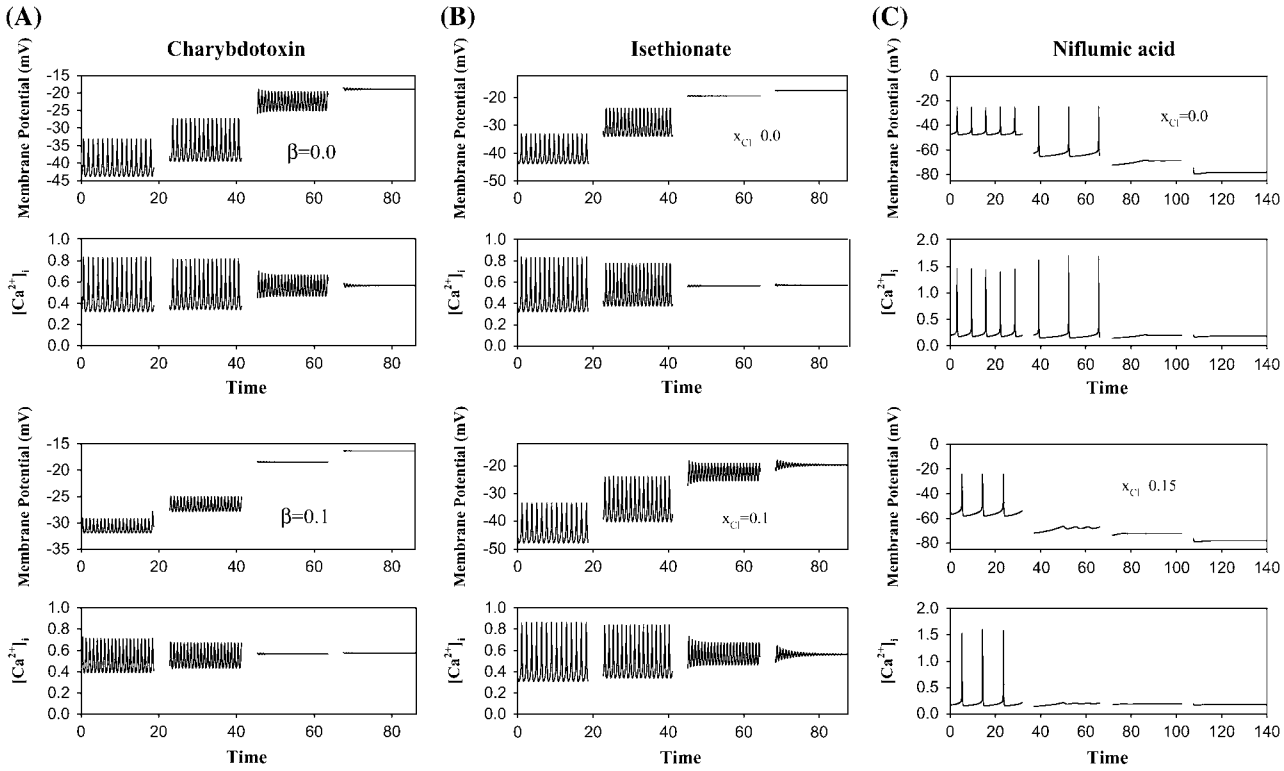

FIGURE 16 (*A*) Simulated action of charybdotoxin for two levels of Ca^{2+}-dependence of K_{Ca} channels. Four stepwise changes in G_K are included in each time series plot ($G_K = 43$, 37, 29, and 25). (*B*) Simulated time series for the action of isethionate for two levels of Ca^{2+} dependence of Cl^- channels. Four stepwise changes in z_{Cl} are included in each time series plot ($\Delta z_{Cl} = 0$, 10, 18, and 20 mV). (*C*) Simulated action of niflumic acid under the same conditions as in *B*. Stepwise changes in G_{Cl} are included in each time series ($G_{Cl} = 65$, 35, 10, and 0, for $A = 0.9$).

specifically dependent on $InsP_3R2$, rather than $InsP_3R1$ or $InsP_3R3$, and only partially suppressed by ryanodine (35,57). Since the RyR and the $InsP_3R$ can thus both contribute to the genesis of oscillatory behavior in vascular smooth muscle cells, we simulated the theoretical contributions of each class of receptor using a monotonically increasing Hill sigmoidal to describe the Ca^{2+} kinetics of the RyR channel and a biphasic dual Hill sigmoidal to describe the Ca^{2+} kinetics of the $InsP_3R$ channel.

Modeling studies confirmed that oscillatory activity could in principle be supported by either channel type, and nullcline analysis provided insights into similarities and differences in their contribution to the dynamics of the system of three differential equations used to model the smooth muscle cell. The general form of the x and y nullclines in simulations separately incorporating the RyR or the $InsP_3R$ was similar at $[Ca^{2+}]_i$ levels <1 μM. In both cases, parameter choices that maintained a high level of $[Ca^{2+}]_{SR}$ generally fell in a nonoscillatory regime, but on increasing channel open probabilities (C_r and C_i) or sensitivity to activation by Ca^{2+} (x_r and x_i) the nullcline intersection translated downward, thereby allowing the emergence of a limit cycle that encircled an unstable equilibrium point, although there was then a progressive decrease in the size of the limit cycle until the system regained stability and oscillations ceased. It follows that activation of either the RyR or the $InsP_3R$ may in theory either promote or suppress oscillatory behavior, according to initial parameter choices. Notably, oscillatory behavior was observed only when their activating Hill slopes (p_r and p_i) were >3, and high values of these coefficients increased the size of the associated limit cycle and reduced oscillation frequency, whereas the Hill exponents for Ca^{2+} release (m_r and m_i) influenced the size of the associated limit cycle but not the existence of oscillatory activity. Thus, the activating mechanisms of the RyR and the $InsP_3R$ appear to be key in generating oscillatory activity. This conclusion is consistent with the reportedly specific ability of the $InsP_3R2$ to support oscillatory behavior, since this subtype possesses an intrinsically higher Hill coefficient for activation by Ca^{2+} than the $InsP_3R1$ or $InsP_3R3$ (40,58,59).

As would be expected, the inactivating component of the $InsP_3R$ kinetics served to maintain Ca^{2+} levels within the sarcoplasmic reticulum store and thereby elevated the positions of the x and y nullclines relative to those associated with the RyR for $[Ca^{2+}]_i > 1$ μM. The Ca^{2+} release phase of the oscillatory cycle, and thus oscillation amplitude, was consequently abbreviated, and there was also an associated reduction in the duration of the store refilling phase that determines oscillation frequency. Decreases in the coefficient h_i of the dual $InsP_3R$ sigmoidal, which mimics the biological

effects of increased [$InsP_3$] on the $InsP_3R$ by causing a leftward shift in the $InsP_3R$ open-probability curve to lower Ca^{2+} levels (39,41,42), accentuated this important difference between the RyR and $InsP_3R$. Although it is often stated in the literature that the biphasic nature of the $InsP_3R$ open-probability curve is crucial for the genesis of oscillatory activity by allowing sequential Ca^{2+}-dependent activation and inactivation of the channel, this assumption was shown to be incorrect in the open system described here, since nullcline analysis indicated that $InsP_3R$-dependent oscillations developed around an unstable equilibrium point with dynamics generically similar to that of the RyR. This situation differs fundamentally from closed-cell models in which there is no influx of extracellular Ca^{2+}. In such systems oscillatory activity has an obligatory dependence on the separation of the timescales that define the kinetics of $InsP_3R$ activation and inactivation rather than the specific form of the quasisteady open probability curve, i.e., whether the curve is biphasic or monotonically increasing (60,61).

The theoretical consequences of manipulating RyR activity in simulations were compared with the effects of ryanodine in rat cerebral arteries. At low concentrations ryanodine increases the open-state probability of the RyR and its sensitivity to Ca^{2+} ions, before locking the channel in an open subconductance state and ultimately causing complete channel closure at high concentrations (28,54,55). Experimentally, 10 μM ryanodine decreased the amplitude of oscillations in membrane potential and $[Ca^{2+}]_i$ and increased vasomotion frequency, and these observations could be simulated by increasing the open probability of the RyR (C_r) or its sensitivity to Ca^{2+} (x_r), consistent with the reported effects of low concentrations of ryanodine. Increasing the leak of Ca^{2+} ions from the store (L), which may be considered as shifting the RyR to an open subconductance state, matched the effects of ryanodine on oscillatory amplitude, whereas vasomotion frequency was essentially unaffected. These findings were shown to apply over a broad range of values of C_r, x_r, and L. Decreasing the coefficient C_r to simulate the closure of the RyR channel reported after administration of high concentrations of ryanodine caused an increase in oscillation amplitude and slowed vasomotion frequency, thus contrasting with the experimental findings. Additional studies would therefore appear necessary to clarify concentration-dependent effects of ryanodine on vasomotion, since the simulated effects of reductions in C_r would be consistent with the reduced frequency and increased amplitude of phenylephrine-induced vasomotion reported in rat small mesenteric arteries after administration of 40 μM ryanodine (12). Further experiments are also required to define the contribution of the $InsP_3R$ to vasomotion in rat arteries since immunostaining has shown that $InsP_3R1$ is the only $InsP_3R$ present in the smooth muscle of the rat aorta and mesenteric artery, whereas in the rat basilar artery there is also expression of $InsP_3R2$, although this is much weaker than that of the $InsP_3R1$ (24). Such findings also suggest that regenerative Ca^{2+} release via the RyR is likely to be the dominant CICR mechanism in rat arteries, since rhythmic activity can be observed in each of the three vessel types (7,8,62), whereas the ability of the $InsP_3R$ to mediate oscillatory behavior is reportedly specific for the $InsP_3R2$ subtype, as noted above.

Numerous studies have provided evidence that crosstalk between the RyR and the $InsP_3R$ can play an important role in Ca^{2+} homeodynamics. In rat portal vein myocytes, for example, positive cooperativity between Ca^{2+}-release sites are thought to enhance local release of Ca^{2+} from a common store, such that opening of the $InsP_3R$ by $InsP_3$ underpins periodic fluctuations in $[Ca^{2+}]_i$ through the recruitment of neighboring RyR channels (57,63). An analogous phenomenon could be simulated in this model by selecting an initial value of C_r that was associated with a high value of $[Ca^{2+}]_{SR}$ in a non-oscillatory regime, and then increasing the value of C_i so as to mimic the progressive superposition of $InsP_3R$-mediated CICR. This strategy resulted in the emergence of an unstable nullcline intersection and associated limit cycle. Alternative possibilities, reported experimentally in colonic and pulmonary artery myocytes, respectively, is that the depletion of the SR Ca^{2+} store that follows the opening of RyR channels attenuates the availability of Ca^{2+} for release via the $InsP_3R$, and vice versa (64,65). Both scenarios could be reproduced by selecting values of C_i and C_r such that the system was in an intermediate oscillatory regime, after which increases in either C_r or C_i, respectively, reduced $[Ca^{2+}]_{SR}$ to a level that was no longer capable of sustaining oscillatory behavior because the nullcline intersection then became stable. The model was also able to reproduce observations that $InsP_3R$-mediated CICR can sometimes appear to dominate oscillatory behavior to the extent that repetitive cytosolic Ca^{2+} spiking is unaffected by administration of ryanodine, e.g., in colonic myocytes (64). Increases in C_r with a fixed value of C_i could thus result in an increase in the oscillation frequency without change in amplitude. This phenomenon occurs because the progressive dominance of the RyR flattens the x and y nullclines for $[Ca^{2+}]_i > 1$ μM, with the overall effect that the oscillatory limit cycle translates downward, but, in contrast to the situation for the RyR alone, is not associated with alterations in amplitude even though there was a progressive fall in $[Ca^{2+}]_{SR}$. By contrast, the theoretical analysis of Eq. 4 suggests that neither the RyR- nor the $InsP_3R$-mediated CICR mechanisms can be a key determinant of mean $[Ca^{2+}]_i$. Indeed, this experimental data indicate that ryanodine can suppress vasomotion in the rat basilar artery without exerting major effects on mean wall $[Ca^{2+}]_i$ or $[Ca^{2+}]_i$ in individual smooth-muscle cells, and ryanodine has also been shown to abolish oscillatory fluctuations in pressure in perfused rabbit arterial segments without affecting mean perfusion pressure (5,17).

Membrane potential and integrated ion fluxes

None of the transmembrane ionic currents incorporated in the model was assigned the status of an independent variable.

Nevertheless, since multiple currents were included in the equation that represented the net rate of change in membrane potential, *dz/dt*, the model was capable of evaluating the effects of pharmacological blockade of the participating membrane fluxes. As shown in Fig. 14, the *dz/dt* curve intersects the horizontal axis at a maximum of three points, which represent possible steady states where oscillations in membrane potential and $[Ca^{2+}]_i$ are abolished, with the central equilibrium point (P2) unstable, but the outer points (P1 and P3) stable, and by plotting families of composite *dz/dt* curves for discrete values of $[Ca^{2+}]_i$, it was possible to delineate the dynamical effects of specific interventions in terms of mean $[Ca^{2+}]_i$ and membrane potential. To illustrate the general behavior of the model, these simulations were performed only for RyR-mediated CICR employing an activation coefficient of 4.

The open system discussed here necessarily requires influx of extracellular Ca^{2+} into the cytosol to maintain oscillatory activity, and this was provided principally by NSCCs and VOCCs. Simulations of the action of the PLC inhibitor U73122 demonstrated theoretically how reduced Ca^{2+} influx via NSCCs after the suppression of DAG formation (modeled as reductions in the coefficient *A*) should decrease mean smooth-muscle $[Ca^{2+}]_i$, promote hyperpolarization, and abolish rhythmic activity, and these findings matched the experimental effects of U73122. For specific values of *A*, simulated blockade of VOCCs by nifedipine (modeled as reductions in the coefficient G_{Ca}) could also result in decreases in $[Ca^{2+}]_i$, promote hyperpolarization and cause a reduction in the amplitude of $[Ca^{2+}]_i$ and membrane potential oscillations, thus matching the experimental effects of nifedipine on these parameters and vessel diameter. In terms of integrated ion fluxes, reductions in G_{Ca} depressed the bell-shaped maximum in the rate of change of membrane potential, *dz/dt*, at membrane potentials close to 0 mV, with a leftward displacement in the P1 stable equilibrium and an associated hyperpolarization that was more marked for depolarized than hyperpolarized states, thus reflecting the open probability of voltage-operated Ca^{2+} channels. Such simulations accord with published data for hamster arterioles exhibiting spontaneous rhythmic activity in vivo, in which nifedipine abolishes vasomotion and causes sustained hyperpolarization and dilatation (66).

The roles of NSCCs and VOCCs were further explored by formal bifurcation analysis, which confirmed that oscillatory behavior was possible only when the net Ca^{2+} flux into the cytosol from the extracellular space via these channels fell within a critical range. A two-dimensional bifurcation diagram for $[Ca^{2+}]_i$ oscillations illustrating the interaction of Ca^{2+} fluxes via NSCCs and VOCCs during manipulation of their respective control parameters (i.e., *A* and G_{Ca}) demonstrated that oscillatory activity arose via a Hopf bifurcation and ceased at a reverse Hopf bifurcation. Nullcline analysis of the model also highlighted the complex interaction between extracellular Ca^{2+} influx and RyR-mediated CICR from stores during variations in *A*, G_{Ca}, and C_r. For combinations of these parameters within the physiological range, the model exhibited oscillatory activity, but for both high and low values of *A* or G_{Ca}, oscillations were suppressed. Experimental evidence that influx of extracellular Ca^{2+} can induce rhythmic activity by specifically activating RyR-mediated CICR has been obtained in rat renal afferent arterioles in which the opening of VOCCs by BAYK-8644 induces pronounced ryanodine-sensitive vasomotion (56).

Vascular smooth-muscle membrane potential is strongly influenced by the balance between K^+ and Cl^- movements, which compete to drive cell potential toward their respective reversal potentials at approximately −95 and −25 mV. Although neither channel was ascribed the status of an independent variable in this three-variable model, simulations allowed a detailed analysis of the role of K^+ and Cl^- channels in the genesis of rhythmic activity and provided insights into the functional consequences of their activation by Ca^{2+} ions. For example, simulating the action of charybdotoxin by reducing the coefficient G_K resulted in depolarization and suppressed oscillatory activity, as observed experimentally. Simulations also indicated that these effects of charybdotoxin, which blocks large- and intermediate-conductance Ca^{2+}-activated K^+ channels, become apparent earlier when the Ca^{2+}-dependence of the K_{Ca} channel is strong. The experimental effects of manipulating smooth-muscle Cl^- fluxes with isethionate or niflumic acid were closely matched by simulations involving stepwise changes in the reversal potential for the Cl^- ion or reductions in G_{Cl}, respectively. Specific consequences of the $[Ca^{2+}]_i$ dependence of Cl^- channels on vasomotion could not be evaluated experimentally, since no specific blockers of such channels are available. However, simulations suggested that an enhanced $[Ca^{2+}]_i$ dependence of the Cl^- channel will extend or reduce the range of oscillatory activity, according to whether the role of such channels is probed with isethionate or niflumic acid, which act in opposing ways to increase and decrease the efflux of Cl^- ions. Importantly, the model was still capable of generating oscillatory behavior when neither channel was conferred with sensitivity to Ca^{2+} (i.e., coefficients β and x_{Cl} were both set to zero), and that the qualitative effects of other superimposed pharmacological interventions were then essentially unchanged, albeit shifted to different parameter ranges. It follows that vasomotion does not have an obligatory requirement for the Ca^{2+} dependence of either K^+ or Cl^- channels, although they may still play an important modulatory role in the genesis of oscillatory activity in the absence of Ca^{2+} sensitivity. Transmembrane K^+ and Cl^- fluxes are governed by the instantaneous difference between their respective reversal potentials and membrane potential, which will necessarily oscillate as a result of ryanodine-sensitive CICR (for example, as a result of Na^+-Ca^{2+} exchange in this model).

In general, the system was found to support sustained oscillatory activity only within a physiological range of $[Ca^{2+}]_i$, $[Ca^{2+}]_{SR}$, and membrane potential, beyond which the behavior of the system collapsed toward stable equilibrium

points via different pathways. Cessation of oscillatory activity may thus result from ''overstimulation'' of the system, when cellular Ca^{2+} influx is high, in which case the concentrations of Ca^{2+} present in the SR store and the cytosol are both too high to support cyclical release of Ca^{2+} from the SR into the cytosol, or ''understimulation'' when Ca^{2+} reuptake is low, in which case the store does not fill sufficiently to support the CICR mechanism. Similarly, strongly hyperpolarizing conditions suppress Ca^{2+} influx via voltage-operated Ca^{2+} channels and strongly depolarizing conditions promote Ca^{2+} influx via this pathway and thus ''understimulate'' or ''overstimulate'' the cell, respectively. These different scenarios were illustrated by the various pharmacological probes employed in this study and were visualized by constructing the phase-space attractor of the system. Thus, U73122, ryanodine, and nifedipine translated the attractor in the direction of the $[Ca^{2+}]_i$ and $[Ca^{2+}]_{SR}$ axes, simultaneously affecting oscillation amplitude and ultimately membrane potential. By contrast, agents that directly affect membrane potential, such as charybdotoxin, isethionate, and niflumic acid, translated the attractor primarily in the direction of the axis depicting membrane potential, thus also affecting oscillatory amplitude and indirectly $[Ca^{2+}]_i$.

Conclusions and future studies

This study has shown that a three-variable model of the smooth muscle cell can provide a close representation of pharmacologically induced changes in smooth-muscle membrane potential and cytosolic $[Ca^{2+}]_i$ during spontaneous vasomotion in isolated rat cerebral arteries. One important assumption of the model is that coupled vascular smooth-muscle cells can synchronize their activity in such a way that vasomotion closely reflects ion movements at the level of the individual cell. To examine this hypothesis in more detail, the model could be extended to define the conditions that permit global entrainment of the intracellular Ca^{2+} waves that occur in individual smooth muscle cells, thereby allowing the emergence of ''macroscopic'' rhythmic activity. Although it is well-established that the synchronization of Ca^{2+} oscillations in vascular smooth muscle cells is dependent on gap junctional communication (6,13,14), it remains unclear whether the dominant intercellular coupling mechanism is electrical or chemical in nature. For completeness, further modeling studies should therefore incorporate the cytoplasmic distribution of stores expressing the RyR and the $InsP_3R$, intracellular and intercellular diffusion of Ca^{2+} ions and $InsP_3$, as well as electrical coupling between adjacent cells. Such studies are likely to suggest experimental approaches that can be tested pharmacologically and thereby clarify the signaling pathways that lead to emergent behavior.

One advantage of this three-variable formulation of the smooth muscle cell is that it focuses on the contribution of a cytosolic oscillator to vasomotion, thus allowing nullcline analysis to provide clear insights into differences and similarities in the dynamics of CICR via the RyR and $InsP_3R$, and the crosstalk that is possible between these Ca^{2+}-release channels. The model also allows the interaction between CICR and membrane transport systems to be investigated in a relatively tractable way, and has provided evidence that the sensitivity of membrane K^+ and Cl^- channels to activation by Ca^{2+} ions is not essential for the existence of rhythmic activity, at the same time demonstrating that the Ca^{2+} sensitivity of such channels determines the parameter ranges over which rhythmic activity becomes manifest. A more complex, compartmentalized model would also allow delineation of how stores located close to the cell membrane might target and activate K_{Ca} and Cl_{Ca} channels in a spatially selective fashion (67–69). Previous experimental studies have, for example, provided evidence that localized RyR-mediated CICR can open K_{Ca} channels in the absence of significant changes in cytosolic $[Ca^{2+}]_i$ (69), although this phenomenon did not appear to be a dominant consideration in this study, since ryanodine did not exert major effects on membrane potential. Since the intracellular Ca^{2+} waves that propagate through individual smooth muscle cells during vasomotion can markedly reduce the frequency of RyR-mediated Ca^{2+} sparks (9), the conditions under which Ca^{2+} oscillations might override and suppress localized elementary events by entraining the CICR mechanism remain to be clarified by modeling and experimental studies.

A particular feature of this model is that the dynamics of a three-variable system is governed by a three-dimensional attractor, thereby allowing full visualization of the relationship between membrane potential, $[Ca^{2+}]_i$, and $[Ca^{2+}]_{SR}$ during simulated pharmacological interventions. The patterns of vasomotion that were observed in nonperfused rat cerebral arteries in this study were relatively simple and readily generated by the three-variable model. However, it should be noted that vasomotion in intraluminally perfused rabbit and rat arterial segments often exhibits more complex nonlinear behavior that is closely associated with chaos, including period-doubling, quasiperiodicity, mixed-mode responses, and intermittency (15–19). One apparent limitation of the this three-variable approach, therefore, is that such generic patterns of chaotic behavior could be simulated only within a very restricted range, when the coefficients of Eqs. 1–3 were assigned values that were generally outside the physiological range (data not shown). By contrast, a four-variable model of the smooth muscle cell, in which the open-state probability of Ca^{2+}-activated K^+ channels was assigned the status of an additional independent dynamical variable, has previously been shown to generate a wide range of nonlinear responses, principally because it allows the coupling of distinct but interacting nonlinear membrane and cytosolic oscillators (each of which requires two independent control variables) (17). It should be noted, however, that it is also possible to generate rich chaotic behavior by coupling nearly identical limit-cycle oscillators such as those developed in this work. Further studies are therefore necessary to compare

the advantages and disadvantages of a coupled-cell approach rather than a single high-order system of differential equations to model vasomotion.

REFERENCES

1. Griffith, T. M. 1996. Temporal chaos in the microcirculation. *Cardiovasc. Res.* 31:342–358.
2. Aalkjaer, C., and H. Nilsson. 2005. Vasomotion: cellular background for the oscillator and for the synchronization of smooth muscle cells. *Br. J. Pharmacol.* 144:605–616.
3. Haddock, R. E., and C. E. Hill. 2005. Rhythmicity in arterial smooth muscle. *J. Physiol.* 566:645–656.
4. Gustafsson, H. 1993. Vasomotion and underlying mechanisms in small arteries. An in vitro study of rat blood vessels. *Acta Physiol. Scand.* 614: 1–44.
5. Griffith, T. M., and D. H. Edwards. 1994. Fractal analysis of role of smooth muscle Ca^{2+} fluxes in genesis of chaotic arterial pressure oscillations. *Am. J. Physiol.* 266:H1801–H1811.
6. Hill, C. E., J. Eade, and S. L. Sandow. 1999. Mechanisms underlying spontaneous rhythmical contractions in irideal arterioles of the rat. *J. Physiol.* 521:507–516.
7. Peng, H., V. Matchkov, A. Ivarsen, C. Aalkjaer, and H. Nilsson. 2001. Hypothesis for the initiation of vasomotion. *Circ. Res.* 88:810–815.
8. Haddock, R. E., and C. E. Hill. 2002. Differential activation of ion channels by inositol 1,4,5-trisphosphate (IP_3)- and ryanodine-sensitive calcium stores in rat basilar artery vasomotion. *J. Physiol.* 545:615–627.
9. Mauban, J. R., C. Lamont, C. W. Balke, and W. G. Wier. 2001. Adrenergic stimulation of rat resistance arteries affects Ca^{2+} sparks, Ca^{2+} waves, and Ca^{2+} oscillations. *Am. J. Physiol.* 280:H2399–H2405.
10. Shaw, L., S. O'Neill, C. J. Jones, C. Austin, and M. J. Taggart. 2004. Comparison of U46619-, endothelin-1- or phenylephrine-induced changes in cellular Ca^{2+} profiles and Ca^{2+} sensitisation of constriction of pressurised rat resistance arteries. *Br. J. Pharmacol.* 141:678–688.
11. Lamboley, M., A. Schuster, J.-L. Beny, and J. J. Meister. 2003. Recruitment of smooth muscle cells and arterial vasomotion. *Am. J. Physiol.* 285:H562–H569.
12. Lamont, C., and W. G. Wier. 2004. Different roles of ryanodine receptors and inositol (1,4,5)-trisphosphate receptors in adrenergically stimulated contractions of small arteries. *Am. J. Physiol.* 287:H617–H625.
13. Matchkov, V. V., A. Rahman, L. M. Bakker, T. M. Griffith, H. Nilsson, and C. Aalkjær. 2006. Analysis of the effects of connexin-mimetic peptides in rat mesenteric small arteries. *Am. J. Physiol.* 291:H357–H367.
14. Chaytor, A. T., W. H. Evans, and T. M. Griffith. 1997. Peptides homologous to extracellular loop motifs of connexin 43 reversibly abolish rhythmic contractile activity in rabbit arteries. *J. Physiol.* 503:99–110.
15. De Brouwer, S., D. H. Edwards, and T. M. Griffith. 1998. Simplification of the quasiperiodic route to chaos in agonist-induced vasomotion by iterative circle maps. *Am. J. Physiol.* 274:H1315–H1326.
16. Stergiopulos, N., C. A. Porret, S. De Brouwer, and J. J. Meister. 1998. Arterial vasomotion: effect of flow and evidence of nonlinear dynamics. *Am. J. Physiol.* 274:H1858–H1864.
17. Parthimos, D., D. H. Edwards, and T. M. Griffith. 1999. Minimal model of arterial chaos generated by coupled intracellular and membrane Ca^{2+} oscillators. *Am. J. Physiol.* 277:H1119–H1144.
18. Parthimos, D., D. H. Edwards, and T. M. Griffith. 2001. Universal scaling properties of type-I intermittent chaos in isolated resistance arteries are unaffected by endogenous nitric oxide synthesis. *Phys. Rev. E.* 64:061906.
19. Parthimos, D., D. H. Edwards, and T. M. Griffith. 2003. Shil'nikov homoclinic chaos is intimately related to type-III intermittency in isolated rabbit arteries: role of nitric oxide. *Phys. Rev. E.* 67:051922.
20. Parthimos, D., K. Osterloh, A. R. Pries, and T. M. Griffith. 2004. Deterministic nonlinear characteristics of in vivo blood flow velocity and arteriolar diameter fluctuations. *Phys. Med. Biol.* 49:1789–1802.
21. Neild, T. O. 1989. Measurement of arteriole diameter changes by analysis of television images. *Blood Vessels.* 26:48–52.
22. Coussin, F., N. Macrez, J. L. Morel, and J. Mironneau. 2000. Requirement of ryanodine receptor subtypes 1 and 2 for Ca^{2+}-induced Ca^{2+} release in vascular myocytes. *J. Biol. Chem.* 275:9596–9603.
23. Lesh, R. E., G. F. Nixon, S. Fleischer, J. A. Airey, A. P. Somlyo, and A. V. Somlyo. 1998. Localization of ryanodine receptors in smooth muscle. *Circ. Res.* 82:175–185.
24. Grayson, T. H., R. E. Haddock, T. P. Murray, R. J. Wojcikiewicz, and C. E. Hill. 2004. Inositol 1,4,5-trisphosphate receptor subtypes are differentially distributed between smooth muscle and endothelial layers of rat arteries. *Cell Calcium.* 36:447–458.
25. Urena, J., T. Smani, and J. Lopez-Barneo. 2004. Differential functional properties of Ca^{2+} stores in pulmonary arterial conduit and resistance myocytes. *Cell Calcium.* 36:525–534.
26. Yang, X. R., M. J. Lin, K. P. Yip, L. H. Jeyakumar, S. Fleischer, G. P. Leung, and J. S. Sham. 2005. Multiple ryanodine receptor subtypes and heterogeneous ryanodine receptor-gated Ca^{2+} stores in pulmonary arterial smooth muscle cells. *Am. J. Physiol.* 289:L338–L348.
27. Fill, M., and J. A. Copello. 2002. Ryanodine receptor calcium release channels. *Physiol. Rev.* 82:893–922.
28. Masumiya, H., P. Li, L. Zhang, and S. R. Chen. 2001. Ryanodine sensitizes the Ca^{2+} release channel (ryanodine receptor) to Ca^{2+} activation. *J. Biol. Chem.* 276:39727–39735.
29. Valdivia, H. H., J. H. Kaplan, G. C. Ellis-Davies, and W. J. Lederer. 1995. Rapid adaptation of cardiac ryanodine receptors: modulation by Mg^{2+} and phosphorylation. *Science.* 267:1997–2000.
30. Goldbeter, A., G. Dupont, and M. J. Berridge. 1990. Minimal model for signal-induced Ca^{2+} oscillations and for their frequency encoding through protein phosphorylation. *Proc. Natl. Acad. Sci. USA.* 87:1461–1465.
31. Sobie, E. A., K. W. Dilly, J. dos Santos Cruz, W. J. Lederer, and M. S. Jafri. 2002. Termination of cardiac Ca^{2+} sparks: an investigative mathematical model of calcium-induced calcium release. *Biophys. J.* 83:59–78.
32. Hinch, R. 2004. A mathematical analysis of the generation and termination of calcium sparks. *Biophys. J.* 86:1293–1307.
33. Abramson, J. J., S. Milne, E. Buck, and I. N. Pessah. 1993. Porphyrin induced calcium release from skeletal muscle sarcoplasmic reticulum. *Arch. Biochem. Biophys.* 301:396–403.
34. Meissner, G., E. Darling, and J. Eveleth. 1986. Kinetics of rapid Ca^{2+} release by sarcoplasmic reticulum. Effects of Ca^{2+}, Mg^{2+}, and adenine nucleotides. *Biochemistry.* 25:236–244.
35. Morel, J. L., N. Fritz, J. L. Lavie, and J. Mironneau. 2003. Crucial role of type 2 inositol 1,4,5-trisphosphate receptors for acetylcholine-induced Ca^{2+} oscillations in vascular myocytes. *Arterioscler. Thromb. Vasc. Biol.* 23:1567–1575.
36. Tu, H., Z. Wang, E. Nosyreva, H. De Smedt, and I. Bezprozvanny. 2005. Functional characterization of mammalian inositol 1,4,5-trisphosphate receptor isoforms. *Biophys. J.* 88:1046–1055.
37. Mak, D. O., S. McBride, and J. K. Foskett. 1998. Inositol 1,4,5-trisphosphate activation of inositol trisphosphate receptor Ca^{2+} channel by ligand tuning of Ca^{2+} inhibition. *Proc. Natl. Acad. Sci. USA.* 95: 15821–15825.
38. Mak, D. O., S. M. McBride, N. B. Petrenko, and J. K. Foskett. 2003. Novel regulation of calcium inhibition of the inositol 1,4,5-trisphosphate receptor calcium-release channel. *J. Gen. Physiol.* 122:569–581.
39. Dufour, J. F., I. M. Arias, and T. J. Turner. 1997. Inositol 1,4,5-trisphosphate and calcium regulate the calcium channel function of the hepatic inositol 1,4,5-trisphosphate receptor. *J. Biol. Chem.* 272:2675–2681.
40. Bezprozvanny, I. 2005. The inositol 1,4,5-trisphosphate receptors. *Cell Calcium.* 38:261–272.
41. Sneyd, J., and M. Falcke. 2005. Models of the inositol trisphosphate receptor. *Prog. Biophys. Mol. Biol.* 89:207–245.
42. Sneyd, J., and J. F. Dufour. 2002. A dynamic model of the type-2 inositol trisphosphate receptor. *Proc. Natl. Acad. Sci. USA.* 99:2398–2403.

43. Li, Y. X., and J. Rinzel. 1994. Equations for InsP3 receptor-mediated $[Ca^{2+}]_i$ oscillations derived from a detailed kinetic model: a Hodgkin-Huxley like formalism. *J. Theor. Biol.* 166:461–473.

44. Hofer, T. 1999. Model of intercellular calcium oscillations in hepatocytes: synchronization of heterogeneous cells. *Biophys. J.* 77:1244–1256.

45. Iino, M., and M. Endo. 1992. Calcium-dependent immediate feedback control of inositol 1,4,5-triphosphate-induced Ca^{2+} release. *Nature.* 360:76–78.

46. Jafri, M. S., J. J. Rice, and R. L. Winslow. 1998. Cardiac Ca^{2+} dynamics: the roles of ryanodine receptor adaptation and sarcoplasmic reticulum load. *Biophys. J.* 74:1149–1168.

47. Terentyev, D., S. Viatchenko-Karpinski, H. H. Valdivia, A. L. Escobar, and S. Gyorke. 2002. Luminal Ca^{2+} controls termination and refractory behavior of Ca^{2+}-induced Ca^{2+} release in cardiac myocytes. *Circ. Res.* 91:414–420.

48. Caroppo, R., M. Colella, A. Colasuonno, A. DeLuisi, L. Debellis, S. Curci, and A. M. Hofer. 2003. A reassessment of the effects of luminal $[Ca^{2+}]$ on inositol 1,4,5-trisphosphate-induced Ca^{2+} release from internal stores. *J. Biol. Chem.* 278:39503–39508.

49. Tanimura, A., and R. J. Turner. 1996. Calcium release in HSY cells conforms to a steady-state mechanism involving regulation of the inositol 1,4,5-trisphosphate receptor Ca^{2+} channel by luminal. *J. Cell Biol.* 132:607–616 $[Ca^{2+}]$.

50. Higo, T., M. Hattori, T. Nakamura, T. Natsume, T. Michikawa, and K. Mikoshiba. 2005. Subtype-specific and ER lumenal environment-dependent regulation of inositol 1,4,5-trisphosphate receptor type 1 by ERp44. *Cell.* 120:85–98.

51. Lytton, J., M. Westlin, S. E. Burk, G. E. Shull, and D. H. MacLennan. 1992. Functional comparisons between isoforms of the sarcoplasmic or endoplasmic reticulum family of calcium pumps. *J. Biol. Chem.* 267: 14483–14489.

52. Albert, A. P., and W. A. Large. 2006. Signal transduction pathways and gating mechanisms of native TRP-like cation channels in vascular myocytes. *J. Physiol.* 570:45–51.

53. Thebault, S., A. Zholos, A. Enfissi, C. Slomianny, E. Dewailly, M. Roudbaraki, J. Parys, and N. Prevarskaya. 2005. Receptor-operated Ca^{2+} entry mediated by TRPC3/TRPC6 proteins in rat prostate smooth muscle (PS1) cell line. *J. Cell. Physiol.* 204:320–328.

54. Rousseau, E., J. S. Smith, and G. Meissner. 1987. Ryanodine modifies conductance and gating behavior of single Ca^{2+} release channel. *Am. J. Physiol.* 253:C364–C368.

55. Buck, E., I. Zimanyi, J. J. Abramson, and I. N. Pessah. 1992. Ryanodine stabilizes multiple conformational states of the skeletal muscle calcium release channel. *J. Biol. Chem.* 267:23560–23567.

56. Takenaka, T., Y. Ohno, K. Hayashi, T. Saruta, and H. Suzuki. 2002. Governance of arteriolar oscillation by ryanodine receptors. *Am. J. Physiol.* 285:R125–R131.

57. Boittin, F. X., N. Macrez, G. Halet, and J. Mironneau. 1999. Norepinephrine-induced Ca^{2+} waves depend on $InsP_3$ and ryanodine receptor activation in vascular myocytes. *Am. J. Physiol.* 277:C139–C151.

58. Miyakawa, T., A. Maeda, T. Yamazawa, K. Hirose, T. Kurosaki, and M. Iino. 1999. Encoding of Ca^{2+} signals by differential expression of IP_3 receptor subtypes. *EMBO J.* 18:1303–1308.

59. Tu, H., Z. Wang, and I. Bezprozvanny. 2005. Modulation of mammalian inositol 1,4,5-trisphosphate receptor isoforms by calcium: a role of calcium sensor region. *Biophys. J.* 88:1056–1069.

60. Li, Y. X., J. Keizer, S. S. Stojilkovic, and J. Rinzel. 1995. Ca^{2+} excitability of the ER membrane: an explanation for IP_3-induced Ca^{2+} oscillations. *Am. J. Physiol.* 269:C1079–C1092.

61. LeBeau, A. P., D. I. Yule, G. E. Groblewski, and J. Sneyd. 1999. Agonist-dependent phosphorylation of the inositol 1,4,5-trisphosphate receptor: a possible mechanism for agonist-specific calcium oscillations in pancreatic acinar cells. *J. Gen. Physiol.* 113:851–872.

62. Freeman, K. A., A. Mao, L. O. Nordberg, J. Pak, and R. J. Tallarida. 1995. The relationship between vessel wall tension and the magnitude and frequency of oscillation in rat aorta. *Life Sci.* 56:PL129–PL134.

63. Gordienko, D. V., and T. B. Bolton. 2002. Crosstalk between ryanodine receptors and IP_3 receptors as a factor shaping spontaneous Ca^{2+}-release events in rabbit portal vein myocytes. *J. Physiol.* 542:743–762.

64. MacMillan, D., S. Chalmers, T. C. Muir, and J. G. McCarron. 2005. IP_3-mediated Ca^{2+} increases do not involve the ryanodine receptor, but ryanodine receptor antagonists reduce IP3-mediated Ca^{2+} increases in guinea-pig colonic smooth muscle cells. *J. Physiol.* 569:533–544.

65. Zheng, Y. M., Q. S. Wang, R. Rathore, W. H. Zhang, J. E. Mazurkiewicz, V. Sorrentino, H. A. Singer, M. I. Kotlikoff, and Y. X. Wang. 2005. Type-3 ryanodine receptors mediate hypoxia-, but not neurotransmitter-induced calcium release and contraction in pulmonary artery smooth muscle cells. *J. Gen. Physiol.* 125:427–440.

66. Bartlett, I. S., G. J. Crane, T. O. Neild, and S. S. Segal. 2000. Electrophysiological basis of arteriolar vasomotion in vivo. *J. Vasc. Res.* 37:568–575.

67. Mironneau, J., S. Arnaudeau, N. Macrez-Lepretre, and F. X. Boittin. 1996. Ca^{2+} sparks and Ca^{2+} waves activate different Ca^{2+}-dependent ion channels in single myocytes from rat portal vein. *Cell Calcium.* 20:153–160.

68. Large, W. A., and Q. Wang. 1996. Characteristics and physiological role of the Ca^{2+}-activated Cl^- conductance in smooth muscle. *Am. J. Physiol.* 271:C435–C454.

69. Jaggar, J. H., V. A. Porter, W. J. Lederer, and M. T. Nelson. 2000. Calcium sparks in smooth muscle. *Am. J. Physiol.* 278:C235–C256.